

SEAL OPTIMIZATION DRIVEN RANDOM FOREST FRAMEWORK FOR ENHANCED ALZHEIMER'S DISEASE CLASSIFICATION

V. HARIPRIYA¹, P. RUTRAVIGNESHWARAN²

¹Research Scholar, Department of Computer Science, Karpagam Academy of Higher Education, India.

¹and Assistant Professor, Department of Computer Technology and Data Science, Sri Krishna Arts and Science College, India.

²Assistant Professor, Department of Computer Science, Karpagam Academy of Higher Education, India.

E-mail: ¹vyharipriya.24@gmail.com, ²rutra20190@gmail.com

ABSTRACT

Alzheimer's Disease remains a progressive neurodegenerative disorder, necessitating early detection for effective intervention. Traditional diagnostic methods face challenges in accuracy, feature selection, and handling high-dimensional neuroimaging data. The purpose of this study is to enhance classification performance by integrating bio-inspired optimization with Machine Learning. A Seal Optimization-driven Random Forest (SO-RF) framework is introduced to refine feature selection, optimize hyperparameters, and improve decision-making in disease classification. The methodology involves leveraging seal-inspired search strategies to enhance the diversity and robustness of the Random Forest model, ensuring balanced precision and recall. The proposed SO-RF model outperforms conventional approaches in classification accuracy, sensitivity, and specificity, demonstrating its effectiveness in reducing false positives and false negatives. Experimental results validate the model's superiority in handling complex medical data, confirming its potential for automated Alzheimer's Disease diagnosis. The optimized classification framework presents a promising solution for advancing computational techniques in neurodegenerative disease detection.

Keywords: *Alzheimer's disease Classification, Bio-Inspired Optimization, Seal Optimization, Random Forest, Feature Selection, Healthcare.*

1. INTRODUCTION

Alzheimer's Disease is a progressive neurodegenerative disease with symptoms of cognitive decline, memory loss, and changes in behavior [1]. It affects mostly old people, who over time lose the capacity to perform everyday tasks [2]. The disease results from abnormal protein depositions in the brain in the form of beta-amyloid plaques and tau tangles, which result in neuronal loss and dysfunction. Over time, the patient suffers from significant cognitive impairment, poor reasoning, and communication difficulties [3]. Brain atrophy worsens with the progress of the disease, causing severe loss of volume in gray matter and impairing neural connections. Early detection and treatment are pivotal in controlling the progress of the disease and enhancing patient outcomes [4]. Alzheimer's Disease is not limited to cognitive impairment and impacts individuals as well as families.

Patients typically experience psychological distress, which in turn results in mood swings, depression, and enhanced dependence on caregivers. The chronic nature of the disease burden emotionally and economically on families in need of long-term care arrangements [5]. With ongoing degeneration of the neurons, the patients face challenge in speech, problem-solving abilities, and the ability to undertake motor functions. The healthcare delivery system is also severely strained from increasing cases and the need to make breakthroughs in early detection and treatment methodology. The disease imposes societal challenges on the health disorder, creating the imperative of effective diagnostic methodologies, individualized therapy, and effective support structures [6].

A number of Alzheimer's Disease effects change the neurological and physiological

functioning of a person. Memory loss is still one of the earliest signs, with patients having trouble remembering recent occurrences while remembering long-term ones for years [7]. Confusion and disorientation worsen as the disease progresses, causing it to be hard to identify known faces and environments. Behavioral symptoms like agitation, paranoia, and social withdrawal make everyday interactions even more complicated [8]. Sleep disturbances usually arise, resulting in abnormal sleep patterns and increased restlessness. The progressive nature of Alzheimer's Disease eventually leads to a total loss of independence, requiring full-time supervision and support in activities of daily living [9].

This research specifically focuses on enhancing early-stage classification of Alzheimer's Disease using bio-inspired optimization within a Random Forest framework. The scope is confined to structural MRI data sourced from the OASIS dataset, assuming consistent imaging quality and accurate clinical labeling. The proposed model does not currently incorporate non-imaging modalities such as PET scans or EEG data. Another assumption is the static nature of the input data, which limits real-time prediction capabilities. While the seal-inspired optimization improves model performance, it may introduce computational overhead during training. Future work may explore dynamic data inputs, real-time adaptability, and inclusion of broader biomarkers to overcome these constraints and further refine Alzheimer's Disease classification accuracy.

Classification and prediction of Alzheimer's Disease continue to be critical in establishing early intervention programs [10]. Different stages of the disease, from mild cognitive impairment to full-blown dementia, demand accurate classification methods. Clinical judgment, cognitive examinations, and neuroimaging form the basis of traditional classification techniques. Subjective human evaluations and overlap of symptoms with other neurodegenerative conditions are major hindrances [11]. Sophisticated computational methods support enhanced classification precision through examination of multimodal information, such as genetic markers, neuroimaging scans, and behavioral patterns. Early-stage classification has the potential to increase the possibilities for timely therapy interventions, dampening disease acceleration and enhancing the quality of patient life [12].

Prediction models utilize large datasets to predict the probability of developing Alzheimer's Disease prior to the onset of clinical symptoms. Risk assessment includes assessing genetic susceptibility, lifestyle, and trends in cognitive function [13]. Predictive analytics use structured and unstructured data to allow for a thorough assessment of disease susceptibility. Machine Learning methods improve prediction accuracy by detecting latent patterns in longitudinal data. Early prediction enables tailored treatment plans, enabling medical professionals to apply preventive measures and cognitive rehabilitation programs [14]. Ongoing advancements in predictive models lead to the improvement of risk assessment models and the optimization of long-term disease management.

Machine Learning application in diagnosis and prognosis of Alzheimer's Disease has grown by leaps and bounds based on advancements in computational powers. Supervised models of learning predict disease phases by categorizing training data, mitigating the ambiguities in diagnoses [15]. Unsupervised learning helps uncover subpopulations of patients to identify patterns in disease course differences. Reinforcement learning tactics provide optimal treatment planning by continually varying interventions with response from the patients [16]. Feature selection methods improve diagnostic precision by ascertaining the most useful biomarkers for classification. The union of Machine Learning with biomedicine speeds up finding probable therapeutic targets, facilitating the development of new treatment approaches [17].

Deep Learning then goes on to transform Alzheimer's Disease detection through the automatic extraction of hierarchical features from high-dimensional data. Convolutional Neural Networks (CNNs) transform neuroimaging scans to identify faint abnormalities associated with disease onset. Recurrent Neural Networks (RNNs) process longitudinal cognitive evaluations, recognizing patterns of deterioration over time [18]. Transfer learning methods optimize model performance through the utilization of pre-trained networks for medical image classification. Generative models mimic disease progression scenarios to inform understanding of underlying mechanisms [19]. The synergy of Deep Learning and biomedical science enhances the accuracy of diagnosis equipment, enabling earlier detection and more precise diagnosis of Alzheimer's Disease.

MRI classification continues to be an anchor in diagnosing Alzheimer's Disease, through high-resolution images that measure structural brain changes. Structural MRI captures cortical thinning, hippocampal atrophy, and enlargement of the ventricles as essential biomarkers of disease development [20]. Functional MRI analyses brain activity patterns and identifies anomalies in neural connections. Automated segmentation methods extract features from MRI imaging, separating normal and diseased brain areas. Deep Learning models improve classification performance through learning spatial and temporal relationships in imaging data[21]. Combination of MRI classification with Machine Learning and Deep Learning enhances the power to detect Alzheimer's Disease in its early stages, facilitating early and specific interventions [22].

Random Forest is a common ensemble learning algorithm used for classification, including diagnosis in medicine. Random Forest creates multiple decision trees with each of them being trained on various subsets of the dataset and their results aggregated to make better predictions. Classification in this model uses a majority vote rule by which individual trees make their prediction and the ultimate output is what was predicted by the most frequent predictions. The strength of Random Forest stems from its capacity to process high-dimensional data and minimize overfitting via random feature selection and bootstrapped sampling. The algorithm is successful in identifying intricate patterns in medical data, hence a useful tool in disease classification [23]. In the case of Alzheimer's Disease, Random Forest is instrumental in processing neuroimaging data, cognitive function tests, and genetic markers towards classifying disease stages. The algorithm separates the relevant features responsible for the decline in cognitive functions, enabling early detection functionality. Through the integration of MRI scan results and clinical information, Random Forest classifies healthy people, mild cognitive impairment patients, and Alzheimer's with great accuracy. Its feature in handling missing values and understanding the importance of the features makes Random Forest a strong candidate for medicine [23]. The application of Random Forest in Alzheimer's research is promoting automated diagnosis, aiding clinical decision-making and enhancing patient management approaches.

Bio-inspired computing is inspired by natural phenomena to address computationally intensive problems [24]. Optimization methods based on biological processes like swarm intelligence, evolutionary algorithms, and neural adaptation are part of this paradigm[25]. These optimization algorithms augment Machine Learning (ML) and Deep Learning (DL) by optimizing model parameters, feature engineering, and hyperparameter tuning, resulting in enhanced accuracy and efficiency. In ML, bio-inspired optimization improves classification, clustering, and regression tasks by optimizing feature representations and decision boundaries [26]. In DL, it improves convergence, avoids overfitting, and optimizes neural network architectures for enhanced generalization. The aim of this work is to incorporate bio-inspired optimization in Alzheimer's Disease prediction to enhance classification performance and facilitate early detection, thereby driving automated diagnosis and personalized treatment plans [27].

1.1. Problem Statement

Alzheimer's Disease remains one of the most challenging neurodegenerative disorders, affecting millions worldwide. Early detection is critical for effective intervention, yet traditional diagnostic methods rely on subjective clinical assessments, often leading to delayed diagnosis and limited treatment efficacy. The complexity of Alzheimer's progression necessitates advanced computational approaches to analyze vast multimodal datasets, including MRI scans, genetic biomarkers, and cognitive assessments. Conventional ML models face challenges in feature selection, model optimization, and handling high-dimensional data, leading to suboptimal classification accuracy.

Existing DL techniques struggle with computational inefficiency, overfitting, and lack of interpretability when applied to Alzheimer's detection. Bio-inspired optimization methods offer a promising solution by mimicking natural intelligence to enhance ML and DL models. However, the integration of such optimization strategies into Random Forest-based classification frameworks remains underexplored. The need for an optimized, robust, and interpretable classification model persists to improve early-stage detection and disease progression analysis. This research addresses these challenges by leveraging bio-inspired optimization techniques to enhance Random Forest models for Alzheimer's Disease

prediction, ensuring accurate, efficient, and early detection, ultimately improving clinical decision-making and patient outcomes. Recent studies [12] emphasize the limitations of current DL and multitask models due to poor generalization and complexity. This study uniquely addresses these gaps by embedding seal-inspired optimization into Random Forest, offering interpretable, adaptive, and performance-driven classification for early Alzheimer's detection.

1.2. Objective and Motivation

The objective of this research is to develop an optimized classification framework for Alzheimer's Disease using bio-inspired techniques integrated with Machine Learning and Deep Learning models. The study focuses on enhancing the accuracy of early-stage detection by refining feature selection, optimizing hyperparameters, and improving classification performance. By leveraging bio-inspired optimization, the goal is to overcome the limitations of conventional models, ensuring efficient handling of high-dimensional neuroimaging and clinical data. Implementing an adaptive optimization strategy will facilitate robust decision-making, reducing diagnostic uncertainties while supporting automated and interpretable predictions.

The motivation behind this work arises from the increasing prevalence of Alzheimer's Disease and the urgent need for reliable early detection methods. Conventional diagnostic approaches rely on subjective evaluations, often leading to delayed interventions and irreversible cognitive decline. Existing computational models lack adaptability, struggling with large-scale medical data complexity. Bio-inspired optimization provides an opportunity to mimic natural intelligence for refining predictive algorithms, ensuring a more precise and efficient classification system. Enhancing Random Forest with these strategies will allow better disease stratification, assisting clinicians in timely and personalized interventions. Addressing these challenges through an optimized computational model will significantly contribute to the advancement of Alzheimer's disease diagnostics and patient care. The research also aims to bridge gaps identified in recent models such as INN-MT and FDCNN-AS by introducing a unified, lightweight, and bio-optimized Random Forest model. This ensures enhanced feature granularity, interpretability, and clinical relevance, contributing to next-generation AI-driven solutions for neurodegenerative disease prediction. The novelty of this study lies in integrating seal-inspired bio-

optimization with Random Forest to enhance Alzheimer's Disease classification. Unlike the conventional methods, the proposed SO-RF framework introduces adaptive optimization at multiple stages feature selection, sampling, and tree construction. Outcome measures such as accuracy, F-measure, FMI, and MCC confirm improved performance and resilience against data imbalance. This layered optimization approach distinguishes the model by offering greater interpretability, robustness, and efficiency in early-stage detection.

2. LITERATURE REVIEW

"Brain Efficiency Model" [28] introduced a network integrating causal relationships with fMRI data for Alzheimer's research. This study designed a causality-driven approach to uncover neural efficiency in brain networks, focusing on how various brain regions communicate during cognitive processes. By employing advanced causal inference techniques, the model analyzed connectivity patterns between regions to identify disrupted interactions associated with Alzheimer's. Unlike traditional correlation-based studies, this approach emphasized the directional impact of one region's activity on another. The methodology utilized functional MRI scans to map neural pathways and incorporated causal algorithms to model the flow of information within the brain. This helped detect key areas where communication breakdowns occur, a hallmark of Alzheimer's progression. The framework also provided insights into compensatory mechanisms employed by the brain to maintain function during early stages of the disease. This causality-driven network has shown potential for improving diagnosis and understanding disease progression by linking structural disruptions to functional deficits.

"Deep Learning Survey" [29] reviewed innovative deep learning models for detecting Alzheimer's using MRI. The paper summarized various architectures such as "Convolutional Neural Networks" (CNNs), "Recurrent Neural Networks" (RNNs), and hybrid frameworks. The focus lay on how these models processed raw MRI data to detect structural abnormalities linked to Alzheimer's. Techniques like transfer learning and attention mechanisms were highlighted for improving classification accuracy with limited data. Preprocessing steps like intensity normalization and skull stripping were discussed for preparing MRI images. The survey covered single-modality and multi-modality approaches that combined MRI with

PET or clinical data to enhance diagnosis. Methods for handling imbalanced datasets, such as “Generative Adversarial Networks” (GANs) for data augmentation, were emphasized. The paper also analyzed the trade-offs between computational cost and diagnostic performance. By providing a comprehensive overview, this work guided future research in Alzheimer’s detection, highlighting gaps like the need for interpretability and robust validation across diverse populations.

“Error Mitigation Framework” [30] proposed a collaborative learning model to predict Alzheimer’s progression with minimal accumulated errors. This framework employed a layered strategy, allowing multiple models to learn from each other iteratively while refining their predictions. Unlike standard ensemble methods, it

focused on error correction at each step, reducing bias and variance.

The design included an innovative weighting mechanism to prioritize reliable predictions, dynamically adjusting model contributions based on performance. Input data, including MRI features and cognitive test scores, were preprocessed and divided across sub-models for independent analysis. Collaborative feedback loops ensured consistent information exchange, improving individual model accuracy. The framework also incorporated adaptive learning rates to optimize prediction in heterogeneous datasets. This system offered a novel way to track disease stages, showing promise for more reliable Alzheimer’s management.

Method Name	Algorithm/ Technique Used	Advantages	Limitations
Brain Efficiency Model [28]	Causal inference with fMRI data	Identified directional connectivity disruptions; enhanced understanding of compensatory mechanisms	Limited to fMRI data; high computational complexity in causal modeling
Deep Learning Survey [29]	Various DL architectures (CNNs, RNNs, GANs)	Comprehensive review guiding future research; highlighted preprocessing and data augmentation	Lack of detailed experimental validation; challenges in model interpretability
Error Mitigation Framework [30]	Collaborative learning with error correction	Reduced bias and variance; robust prediction of disease progression	Computational overhead due to iterative learning; limited scalability
Fibonacci-Based Analysis [31]	Fibonacci sequence for feature extraction in MRI	Improved feature selection and computational efficiency; fine-grained spatial analysis	Applicability limited to specific imaging features; moderate generalization
Texture-Based Classifier [32]	SVM with texture feature extraction	Captured subtle structural irregularities; reliable classification	Dependency on feature extraction algorithms; moderate scalability
Color-Fusion System [33]	Deep learning with multimodal color-coded visualization	Enhanced interpretability; effective tracking of disease progression	Computationally intensive; reliance on high-quality multimodal data
Multi-Scale Framework [34]	Multi-scale CNN + LSTM	Captured granular insights across modalities; addressed heterogeneity	Complex architecture; requires substantial labeled data
Clinical Record Classifier [35]	RNN with attention mechanism	Effective use of longitudinal EHRs; holistic diagnostic approach	Dependent on clinical data availability and consistency
Next-Gen Diagnostics [36]	Self-supervised learning, CNN, GNN	Robust feature representations; domain-specific pretraining improved generalizability	High model complexity; extensive computational resources required

EEG Ensemble Classifier [37]	Hybrid deep ensemble learning	Strong classification performance with non-invasive EEG signals	Dependency on signal preprocessing; computational overhead due to ensembles
ANALYZE-AD [38]	Comparative analysis of AI techniques	Identified gaps and strengths in current methods; guided robust diagnostic development	Limited to literature review; lacks implementation of proposed techniques
Multimodal Hybrid Model [39]	PCA, random forests, SVM for multimodal integration	Holistic view of disease progression; improved diagnostic accuracy	High complexity in feature alignment; moderate scalability
Alzh-Net [40]	Residual CNN with spatial attention	Efficient processing of MRI data; robust early-stage diagnosis	Limited to MRI data; challenges in handling multimodal datasets
Graph-Regularized Selector [41]	Graph-based regularized feature selection	Extracted meaningful patterns; effective multimodal fusion	Sensitivity to noise in graph modeling; requires prior domain knowledge
Robust-PCA EEG Classifier [42]	Robust PCA and random forest	Reduced noise; cost-effective diagnostic potential using EEG	Limited to EEG signals; lower spatial resolution compared to imaging
FDCNN-AS [43]	Federated Deep Convolutional Neural Network (FDCNN)	Ensures data privacy - Adapts to different age groups - Enhances detection accuracy.	High computational cost - Communication overhead - Sensitive to non-IID data.
INN-MT [44]	Multi-Task Learning (MTL) with Neural Network	Improves classification accuracy - Reduces overfitting - Enhances generalization.	Complex implementation - Higher resource demand - Requires balanced task learning.

Table 1: Literature Review

“Fibonacci-Based Analysis” [31] explored Alzheimer’s detection using MRI and a Fibonacci-inspired model. FiboNeXt applied the Fibonacci sequence for feature extraction, leveraging its mathematical properties to identify significant imaging patterns. The model divided brain MRI into segments and analyzed them hierarchically using Fibonacci ratios, uncovering fine-grained spatial changes in brain structure. These method enhanced feature selections, focusing on regions linked to early-stage Alzheimer’s, like the hippocampus and temporal lobes. A neural network classifier, trained on the extracted features, provided robust differentiation between healthy and diseased samples. Cross-validation techniques ensured model reliability, and performance was benchmarked against conventional methods. The innovative use of Fibonacci principles reduced computational complexity while improving diagnostic precision.

“Texture-Based Classifier” [32] utilized machine learning to classify Alzheimer’s disease by analyzing texture features in MRI. Texture metrics, including coarseness, contrast, and homogeneity,

were extracted from brain scans to characterize structural irregularities. Feature selection algorithms, such as Relieff, identified the most relevant parameters for distinguishing Alzheimer’s stages. The classification process employed “Support Vector Machines” (SVMs) with a radial basis function kernel, optimized through hyperparameter tuning. The approach demonstrated efficiency in capturing subtle textural changes, particularly in the grey matter. Cross-validation and statistical analyses confirmed its reliability, making it a promising tool for Alzheimer’s detection.

“Color-Fusion System” [33] developed a novel visualization technique combining multimodal data and deep learning for Alzheimer’s longitudinal studies. The system employed color-coding to integrate structural MRI, PET scans, and clinical records, enhancing interpretability. The visualization framework mapped disease progression by dynamically updating colors to represent changes in biomarkers over time. Deep learning algorithms processed multimodal inputs, extracting spatial, temporal, and contextual features. These features were fused into a unified

model, providing comprehensive insights into brain atrophy patterns and metabolic activity. The system streamlined longitudinal analysis, enabling clinicians to track subtle cognitive and structural changes with ease. The integration of multimodal data significantly improved diagnostic accuracy and highlighted correlations between clinical and imaging biomarkers.

“Multi-Scale Framework” [34] introduced a deep learning model integrating multi-scale features from multimodal data for Alzheimer’s diagnosis. The framework combined MRI, PET, and genetic information to capture structural, functional, and molecular changes. Multi-scale processing analyzed data at various resolutions, ensuring granular insights into brain alterations. A “Convolutional Neural Network” (CNN) extracted spatial features, while a “Long Short-Term Memory” (LSTM) network modeled temporal dependencies. A fusion layer synthesized outputs from multiple modalities, optimizing feature interactions. The framework addressed challenges in data heterogeneity and imbalanced datasets through transfer learning and augmentation. This approach delivered robust classification performance, enhancing early detection and disease staging.

“Clinical Record Classifier” [35] utilized deep learning to diagnose Alzheimer’s using electronic health records (EHRs). The model processed longitudinal clinical data, including cognitive scores, medication history, and lab results, to identify patterns indicative of Alzheimer’s. A “Recurrent Neural Network” (RNN) architecture analyzed temporal trends, while an attention mechanism highlighted key predictors. The system integrated demographic and comorbidity information, enabling a holistic diagnostic approach. Preprocessing steps ensured data consistency by addressing missing values and standardizing input formats. The model outperformed traditional rule-based systems by capturing subtle correlations across heterogeneous clinical records, supporting reliable Alzheimer’s diagnosis and treatment planning.

“Next-Gen Diagnostics” [36] employed advanced deep learning techniques to refine Alzheimer’s early detection. The study incorporated hybrid architectures combining convolutional layers and “Graph Neural Networks” (GNNs) to analyze spatial and relational data from MRI and PET scans. The model introduced an

innovative self-supervised learning module to address limited labeled data. Contrastive learning extracted robust feature representations by maximizing differences between healthy and diseased samples. Transfer learning with domain-specific pretraining improved model generalizability across diverse datasets. The framework achieved superior performance in identifying early-stage Alzheimer’s, laying a foundation for more precise and accessible diagnostic tools.

“EEG Ensemble Classifier” [37] presented a hybrid deep ensemble learning approach for Alzheimer’s classification using EEG data. The model combined “Convolutional Neural Networks” (CNNs) for spatial feature extraction and “Recurrent Neural Networks” (RNNs) for temporal analysis. Ensemble learning incorporated multiple classifiers, including decision trees and “Support Vector Machines” (SVMs), to enhance robustness. The hybrid model utilized wavelet transforms to preprocess EEG signals, isolating frequency bands critical to Alzheimer’s diagnosis. A weighted voting mechanism optimized final predictions by integrating outputs from diverse classifiers. This approach demonstrated strong classification performance, highlighting its applicability in non-invasive Alzheimer’s detection.

“ANALYZE-AD” [38] conducted a thorough comparison of diverse artificial intelligence methodologies to identify effective techniques for early Alzheimer’s detection. The study reviewed supervised and unsupervised learning models, emphasizing their performance on structural MRI, PET scans, and clinical data. Each model’s ability to handle imbalanced datasets, reduce feature dimensionality, and enhance interpretability was assessed. Novel frameworks such as graph-based neural networks and attention-based mechanisms were included for their capability to capture complex relationships in multimodal datasets. Transfer learning and data augmentation were explored to improve generalization across different cohorts. The analysis identified the strengths and weaknesses of various approaches, offering guidance for developing robust diagnostic systems.

“Multimodal Hybrid Model” [39] integrated data from structural MRI, PET scans, and cognitive assessments to detect Alzheimer’s disease with high precision. The model used a hybrid approach combining feature extraction,

selection, and classification techniques. “Principal Component Analysis” (PCA) reduced dimensionality, while random forests and “Support Vector Machines” (SVM) formed the ensemble classification layer. The model aligned extracted features from different modalities to capture complementary information about brain structure and function. By combining imaging biomarkers with clinical and cognitive data, the framework provided a holistic view of disease progression. This method achieved improved diagnostic accuracy and demonstrated adaptability to complex datasets.

“Alzh-Net” [40] proposed a “Convolutional Neural Network” (CNN) specifically designed for analyzing MRI data to diagnose Alzheimer’s disease. The model incorporated residual connections to preserve critical features during processing, ensuring robust learning from complex brain imaging data. A preprocessing pipeline standardized MRI scans, enhancing contrast and eliminating noise. The network utilized spatial attention mechanisms to focus on key regions such as the hippocampus and temporal lobes. Batch normalization and dropout layers minimized overfitting and ensured generalization across datasets. The method demonstrated high efficiency in diagnosing mild cognitive impairment and early-stage Alzheimer’s disease, facilitating early medical intervention.

“Graph-Regularized Selector” [41] introduced a feature selection method leveraging graph-based regularization to enhance Alzheimer’s classification using multimodal data. This approach employed multi-level graphs to model relationships among imaging, cognitive, and genetic data. Feature relevance was assessed by integrating local and global structural correlations. Robust optimization techniques addressed noise and outliers, ensuring stable feature selection. The selected features were fed into “Support Vector Machines” (SVMs) for classification. Cross-validation confirmed the method's capacity to extract meaningful patterns while maintaining low computational complexity. The framework achieved effective multimodal fusion, advancing Alzheimer’s diagnostic tools.

“Robust-PCA EEG Classifier” [42] utilized robust principal component analysis (PCA) to extract features from EEG signals for Alzheimer’s disease classification. This technique decomposed EEG data into low-rank and sparse

components, isolating relevant patterns while reducing noise. Wavelet transformation and frequency domain analysis enhanced signal preprocessing. The extracted features captured brain connectivity and functional abnormalities associated with Alzheimer’s. A random forest classifier identified Alzheimer’s and healthy controls with significant accuracy. This method showcased the potential of non-invasive EEG data and feature decomposition techniques in developing cost-effective diagnostic solutions for Alzheimer’s disease. Bio-inspired are being applied in different research to attain better results [43]-[79].

“FDCNN-AS” [80] presents a federated deep convolutional neural network framework for Alzheimer’s disease detection across various age groups. This model utilizes federated learning to train on distributed datasets while maintaining data privacy, ensuring collaborative learning without centralized data sharing. By employing deep convolutional architectures, the network captures essential biomarkers from brain imaging data, enhancing classification accuracy. The method adapts to age-related variations in Alzheimer’s progression, improving personalized detection strategies. Through advanced feature extraction and secure distributed learning, this approach offers a robust solution for early diagnosis and monitoring of the disease, catering to different age demographics while addressing privacy concerns in medical data analysis. “INN-MT” [81] introduces a neural network framework integrating multi-task learning to enhance Alzheimer’s disease classification. This approach enables simultaneous learning of multiple related tasks, improving model generalization and accuracy. The network processes diverse features from brain imaging data, identifying distinct patterns associated with different stages of the disease. By leveraging shared representations across tasks, the model enhances early diagnosis and disease progression monitoring. This method optimizes computational efficiency while maintaining high predictive performance, making it a valuable tool for Alzheimer’s detection and classification in clinical applications.

3. SEAL OPTIMIZATION-INSPIRED RANDOM FOREST (SO-RF)

SO-RF combines the principles of seal-inspired optimization and the Random Forest algorithm to enhance the model's performance in complex prediction tasks such as Alzheimer’s detection. Seal-inspired optimization is based on seals' efficient navigation and decision-making in

dynamic environments, which can be applied to fine-tune the hyperparameters or enhance feature selection in Random Forest. Fig1. Depicts the overall framework of SO-RF.

3.1. Initialization of Seal-Inspired Parameters

Seal optimization-based mechanisms emulate the behaviours of seals in complex navigation and foraging.

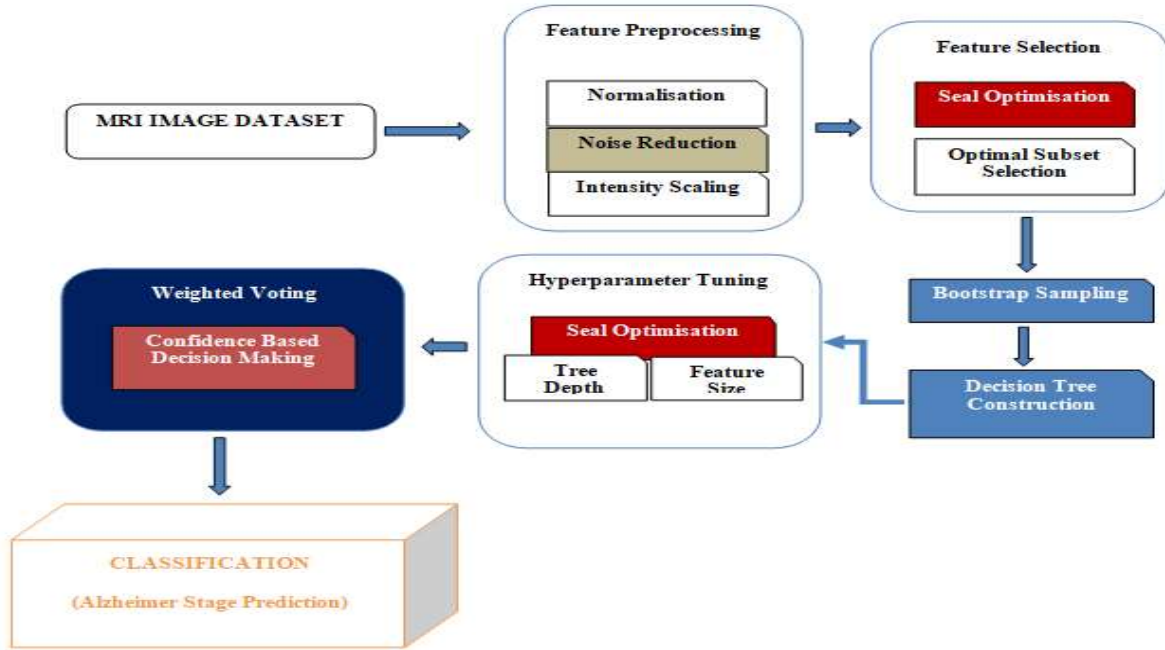


Fig1. Overall framework of SO-RF

These behaviours are modelled mathematically to establish a robust foundation for optimization. The initialization of seal-inspired parameters involves defining the variables and equations necessary to guide the algorithm. The process ensures a strong basis for subsequent steps in the algorithm, particularly for feature selection, tree construction, and hyperparameter tuning.

Parameter Definitions and Initialization

In seal-inspired optimization, key parameters include search agents, navigation steps, energy levels, and the fitness of potential solutions. These parameters are initialized using specific mathematical formulations that mimic seal behaviour. The position of the seal in the search space is represented as Eq.(1).

$$S_i^t = S_i^{t-1} + \alpha \cdot (\beta \cdot R - \gamma \cdot P) \quad (1)$$

where, S_i^t denotes the position of the i -th seal at iteration t . The variable R represents the random exploration direction, and P indicates the prey's position. Parameters α , β , and γ are the navigation, randomness, and convergence rates, respectively. To ensure that seals navigate efficiently, the energy decay function is defined as Eq.(2).

$$E_t = E_{max} \cdot \exp(-\delta \cdot t) \quad (2)$$

The term E_t describes the energy level at iteration t , δ is the energy decay constant, and E_{max} is the initial energy level. This formulation ensures realistic decay over time, aligning with seal foraging efficiency.

Exploration and Exploitation Balance

The behaviour of seals requires a balance between exploration (searching for new areas) and exploitation (intensifying around promising solutions). The exploration-exploitation control is established which is represented mathematically in Eq.(3).

$$\psi = \sigma \cdot \sin(\omega \cdot t) + \tau \quad (3)$$

ψ controls the balance, σ and τ are parameters governing the oscillation amplitude and bias, while ω represents the frequency of oscillation over iterations.

The velocity of seal movement within the search space is described as expressed mathematically in Eq.(4).

$$V_i^{t+1} = \eta \cdot V_i^t + \zeta \cdot (S_g^t - S_i^t) \quad (4)$$

where, V_i^{t+1} represents the updated velocity of the i -th seal, η is the inertia coefficient, and ζ denotes the adjustment factor based on the global best position S_g^t .

Dynamic adaptation of parameters

The initialization step also incorporates mechanisms for dynamically adapting the parameters based on feedback from the optimization process. The adaptive convergence parameter is mathematically expressed in Eq.(5).

$$\mu_t = \mu_0 \cdot \left(1 - \frac{t}{T}\right) \quad (5)$$

Where μ_t is the convergence parameter at iteration t , μ_0 is the initial convergence value, and T is the total number of iterations. This dynamic adaptation ensures the algorithm transitions smoothly between the exploration and exploitation phases.

Seal swarm density, a critical factor for collective navigation, is expressed as Eq.(6).

$$D_t = \frac{\sum_{i=1}^N \exp(-k \cdot \|S_i^t - S_c^t\|)}{N} \quad (6)$$

The swarm density D_t depends on the positions of all seals S_i^t , the central position S_c^t , and the dispersion constant k .

Energy and distance considerations

Seals rely on energy and distance constraints to optimize their movement. The energy-distance function for position updates is formulated as shown in Eq.(7).

$$U_i^t = \lambda \cdot S_i^t + \nu \cdot (P - S_i^t) \quad (7)$$

The position update factor U_i^t combines the current position S_i^t and the prey position P with weights λ and ν , corresponding to local and global contributions.

The scaling factor captures the adaptability in dynamic environments which is represented mathematically in Eq.(8).

$$\theta_t = \theta_{min} + (\theta_{max} - \theta_{min}) \cdot \frac{t}{T} \quad (8)$$

This scaling factor θ_t ensures a gradual shift from exploration-dominant to exploitation-dominant strategies.

3.2. Feature Selection Process

The feature selection process in SO-RF leverages the seal-inspired optimization framework to identify the most significant features for model training. This step optimizes feature selection by mimicking seals' ability to focus on critical targets

in dynamic environments. The mechanism ensures that only the most relevant features contribute to decision-making, reducing noise and enhancing overall model performance.

Feature scoring and initialization

Feature scoring assigns important values to each feature based on its contribution to the objective function. Seal-inspired behaviour drives this scoring by balancing local exploration and global exploitation of the feature space. The scoring function is defined as Eq.(9).

$$F_i = \frac{\sum_{j=1}^M \phi_j \cdot G_{ij}}{\sum_{j=1}^M \phi_j} \quad (9)$$

where, F_i denotes the important score of feature i . The parameter G_{ij} represents the gradient contribution of feature i across all M samples, while ϕ_j is the corresponding weight assigned to sample j , reflecting its significance.

Each feature's initial weight is set dynamically which is represented mathematically in Eq.(10).

$$\phi_i^t = \phi_i^{t-1} \left(1 + \frac{\eta}{1 + \|X_i - P\|}\right) \quad (10)$$

where, ϕ_i^t is the weight of feature i at iteration t . The term η controls the influence of proximity to the target position P , and X_i represents the position of feature i in the search space.

Adaptive feature selection strategy

The adaptive strategy uses energy levels inspired by seal behaviour to prioritize features dynamically. The selection probability of a feature is defined as Eq.(11).

$$P_i = \frac{\exp(-\xi \cdot F_i)}{\sum_{k=1}^N \exp(-\xi \cdot F_k)} \quad (11)$$

The parameter P_i represents the probability of selecting feature i , with N being the total number of features. The scaling factor ξ adjusts the sensitivity of the selection process to feature scores. The adaptive cutoff threshold for selected features is given as shown in Eq.(12).

$$\Theta = \Theta_{max} \cdot \exp\left(-\rho \cdot \frac{t}{T}\right) \quad (12)$$

Θ is the threshold at iteration t , Θ_{max} is the initial maximum threshold, ρ is the decay rate, and T is the total number of iterations. This ensures the gradual refinement of selected features over time.

Movement dynamics in feature space

Seals' coordinated movement in the feature space is emulated to improve feature selection. The update rule for feature positions is formulated as Eq.(13).

$$X_i^{t+1} = X_i^t + \lambda \cdot (X_g - X_i^t) + \zeta \cdot R \quad (13)$$

The position X_i^{t+1} of feature i at iteration $t + 1$ depends on its previous position X_i^t , the global best position X_g , and a random exploration vector R . Parameters λ and ζ balance exploitation and exploration.

Feature stability over iterations is quantified using a convergence factor is defined as Eq.(14).

$$C_i^t = \alpha \cdot C_i^{t-1} + (1 - \alpha) \cdot |F_i^t - F_i^{t-1}| \quad (14)$$

The convergence factor C_i^t ensures that features stabilizing quickly are prioritized, where α controls the influence of historical stability.

Feature optimization using seal behaviour

The final selection of features integrates feedback from multiple iterations, optimizing the subset to balance diversity and relevance. The optimized subset S is determined as Eq.(15).

$$S = \{i: F_i \geq \Theta \text{ and } P_i > \tau\} \quad (15)$$

where, S includes features meeting the importance threshold Θ and having a selection probability P_i greater than a predefined threshold τ . This ensures the chosen features align closely with the optimization objectives.

3.3. Bootstrap Sampling

Bootstrap sampling involves generating diverse subsets of data to train individual decision trees within the Random Forest algorithm. The seal-inspired optimization in SO-RF enhances the traditional bootstrap process by introducing dynamic sampling strategies influenced by seal foraging behaviour, ensuring diverse and balanced subsets. This step strengthens the model's robustness and generalization by leveraging optimized sampling mechanisms.

Dynamic sampling rate

The dynamic sampling rate, inspired by seals' adaptive exploration strategies, is defined as Eq.(16).

$$R_t = R_{min} + (R_{max} - R_{min}) \cdot \sin\left(\frac{\pi \cdot t}{T}\right) \quad (16)$$

The variable R_t represents the sampling rate at iteration t , R_{min} and R_{max} denote the minimum and maximum sampling rates, and T is the total number of iterations. This oscillatory mechanism ensures varied sampling patterns, balancing exploration and exploitation over time.

The number of samples selected from the dataset is expressed as Eq.(17).

$$N_t = [R_t \cdot N_{total}] \quad (17)$$

where N_t is the number of samples at iteration t , R_t is the sampling rate, and N_{total} is the total number of available samples. This formula ensures proportional sampling based on the dynamically adjusted rate.

Weighting of Data Instances

Seal-inspired strategies assign weights to data instances to prioritize informative samples. The instance weight w_i^t at iteration, t is computed as Eq.(18).

$$w_i^t = \frac{1}{1 + \exp(-k \cdot f_i)} \quad (18)$$

where, w_i^t represents the weight; for instance i , κ controls the steepness of the weighting function, and f_i is the fitness score of the instance, reflecting its relevance.

To maintain a balance in instance selection, the normalized weight for sampling is defined as Eq.(19).

$$\hat{w}_i^t = \frac{w_i^t}{\sum_{j=1}^{N_{total}} w_j^t} \quad (19)$$

The normalized weight \hat{w}_i^t ensures that the sum of weights across all instances equals one, facilitating probabilistic sampling.

Selection probability adjustment

The selection probability for each data instance integrates feedback from its weight and prior selection frequency. The probability P_i^t for instance i is calculated as defined in Eq.(20).

$$P_i^t = \frac{\hat{w}_i^t}{1 + \lambda \cdot freq_i^t} \quad (20)$$

In this equation, P_i^t accounts for the normalized weight \hat{w}_i^t , the prior selection frequency $freq_i^t$, and λ , which balances between informative selection and diversity.

Diversity maximization in sampling

Diversity among sampled subsets is enhanced by seal-inspired dispersion. The dispersion factor δ_t determines the spread of selected instances and is expressed as Eq.(21).

$$\delta_t = \delta_{min} + (\delta_{max} - \delta_{min}) \cdot \cos\left(\frac{\pi \cdot t}{2T}\right) \quad (21)$$

The term δ_t adjusts the dispersion based on iteration t , with δ_{min} and δ_{max} as bounds, this ensures broad coverage of the feature space in early iterations, narrowing it down as optimization progresses.

Sampling update rule

An update rule inspired by seal swarm dynamics is applied to refine the sample set. The

updated position of a selected instance is computed as Eq.(22).

$$X_i^{t+1} = X_i^t + \sigma \cdot (X_c - X_i^t) + \omega \cdot R_t \quad (22)$$

where, X_i^{t+1} denotes the new position of instance i , X_c is the centroid of the selected samples, R_t represents a random perturbation, and σ and ω balance convergence and diversity.

3.4. Feature Subset Selection Per Tree

Feature subset selection per tree ensures diversity and relevance in the construction of decision trees. In SO-RF, this process is guided by seal-inspired optimization principles, enabling the selection of optimal feature subsets for each tree. This step enhances the overall robustness and accuracy of the Random Forest by ensuring that the chosen features are dynamically aligned with the optimization objectives.

Dynamic feature scoring

Feature subset selection begins with assigning scores to features based on their contribution to learning. The dynamic feature scoring is represented as Eq.(23).

$$S_f^t = S_f^{t-1} + \beta \cdot \frac{G_f^t}{\|G_f^t\|} \quad (23)$$

Here, S_f^t denotes the score of feature f at iteration t . The term G_f^t represents the gradient of the feature at t , normalized to unit magnitude. The coefficient β regulates the influence of the gradient on the score update.

Feature selection probability

Using the feature scores, the probability of selecting a feature is defined dynamically to prioritize informative features. The selection probability for feature f is computed as Eq.(24).

$$P_f = \frac{S_f^t}{\sum_{j=1}^F S_j^t} \quad (24)$$

where, P_f denotes the probability of selecting feature f , S_f^t is its score at iteration t , and F is the total number of features. This normalization ensures that probabilities are proportional to feature importance.

Diversity enhancement in feature subsets

A dispersion mechanism inspired by seal behaviour is applied to maximize diversity among trees. The dispersion factor for feature subsets is expressed as Eq.(25).

$$D_f = \frac{1}{1 + \exp(-\lambda \cdot \|V_f - C\|)} \quad (25)$$

The term D_f represents the dispersion value for feature f , λ adjusts the steepness of the function,

V_f is the vector representation of feature f , and C is the centroid of selected features in the subset.

Subset optimization

The optimization of feature subsets is achieved by selecting features with the highest combined scores from importance and diversity. The optimization objective is defined as Eq.(26).

$$O_f = \alpha \cdot P_f + (1 - \alpha) \cdot D_f \quad (26)$$

where, O_f is the optimization value for feature f , α is the weight balancing importance and diversity, P_f is the selection probability, and D_f is the dispersion factor.

Feature subset allocation

The final selection of features for a tree is determined by solving a maximization problem over the optimization values are expressed mathematically in Eq.(27).

$$F_t = \arg \max_{f \in F} (O_f), \text{ where } |F_t| \leq k \quad (27)$$

where, F_t is the subset of features selected for the tree at iteration t , and k is the predefined maximum number of features per tree. This ensures that the subset includes only the most optimized features.

3.5. Dynamic Node Splitting Criterion in SO-RF

The Dynamic Node Splitting Criterion in SO-RF employs seal-inspired optimization principles to determine optimal split points in decision trees. This mechanism ensures that splits maximize information gain while maintaining diversity and robustness in the decision process. The adaptive nature of the criterion enhances the tree's performance in handling complex and noisy data distributions.

Information gain optimization

The criterion for a node split begins with the calculation of information gain, defined as Eq.(28).

$$IG(X, \theta) = H(X) - \sum_{k=1}^K \frac{|X_k|}{|X|} H(X_k) \quad (28)$$

Where, $IG(X, \theta)$ represents the information gain for a feature X at split point θ . The term $H(X)$ is the entropy of the parent node, and $H(X_k)$ represents the entropy of the k -th child node, with $|X_k|$ denoting the number of samples in the child node and $|X|$ the total samples in the parent node. The Entropy $H(X)$ is calculated as represented mathematically in Eq.(29).

$$H(X) = - \sum_{i=1}^C p_i \log_2(p_i) \quad (29)$$

The term p_i indicates the proportion of samples in class i at the node, and C is the total number of classes. This equation quantifies the impurity of the node.

Adaptive gini index for splitting

The Gini index is adapted using seal-inspired dynamics to prioritize nodes with a balanced class distribution. The adaptive Gini index is expressed as Eq.(30).

$$G(X, \theta) = \sum_{i=1}^c p_i(1 - p_i) + \delta \cdot \|X - \theta\| \quad (30)$$

The term $G(X, \theta)$ combines the traditional Gini index with a penalty term, where δ regulates the impact of the distance $\|X - \theta\|$ between the feature values and split point. This adaptation ensures optimal splits while accounting for feature variability.

Weighted variance reduction

In regression tasks, the splitting criterion uses weighted variance reduction is expressed mathematically in Eq.(31).

$$VR(X, \theta) = \sigma^2(X) - \sum_{k=1}^K \frac{|X_k|}{X} \sigma^2(X_k) \quad (31)$$

The term $VR(X, \theta)$ represents the variance reduction, where $\sigma^2(X)$ is the variance of the parent node, and $\sigma^2(X_k)$ denotes the variance of the k -th child node. This equation ensures that the split minimizes variance across child nodes.

Variance is calculated as expressed mathematically in Eq.(32).

$$\sigma^2(X) = \frac{1}{|X|} \sum_{i=1}^{|X|} (x_i - \bar{x})^2 \quad (32)$$

where, $\sigma^2(X)$ is the variance, x_i are the feature values, and \bar{x} is their mean. This formulation ensures that the split minimizes dispersion in the resulting nodes.

Seal-inspired split selection

The optimal split is selected using a seal-inspired optimization function is expressed mathematically in Eq.(33).

$$\Theta^* = \arg \max_{\theta} (\alpha \cdot IG(X, \theta) + \beta \cdot VR(X, \theta) - \gamma \cdot G(X, \theta)) \quad (33)$$

The term Θ^* denotes the optimal split point. Parameters α , β , and γ balance the contributions of information gain, variance reduction, and the adaptive Gini index. This function ensures that splits optimize classification and regression objectives simultaneously.

Dynamic thresholding for splits

A dynamic threshold adjusts the sensitivity of split selection over iterations are expressed mathematically in Eq.(34).

$$\lambda_t = \lambda_0 \cdot \left(1 - \frac{t}{T}\right) \quad (34)$$

where, λ_t is the threshold at iteration t , λ_0 is the initial threshold, and T is the total number of iterations. This dynamic adjustment refines the splits as the algorithm progresses.

Seal-swarm feedback mechanism

The feedback from neighbouring nodes influences split selection dynamically. This is expressed as Eq.(35).

$$\Phi_t = \Phi_{t-1} + \eta \cdot (\Phi_{best} - \Phi_{t-1}) \quad (35)$$

where, Φ_t represents the updated feedback at iteration t , Φ_{best} is the best feedback observed, and η regulates the influence of the input on the current iteration. This ensures continuous improvement in split quality.

3.6. Construction of Diverse Trees

The construction of diverse trees in SO-RF utilizes seal-inspired optimization principles to ensure that each tree contributes unique decision-making capabilities to the ensemble. This step emphasizes diversity to reduce overfitting and enhance generalization. Dynamic strategies balance exploration and exploitation in tree construction, guided by seal-like adaptive behaviour.

Dynamic sampling for tree diversity

Diverse trees are constructed using unique sampling rates and weights during bootstrap sampling. The weight-adjusted sampling probability for a data instance is defined as Eq.(36)

$$P_i^t = \frac{w_i^t}{\sum_{j=1}^N w_j^t} \quad (36)$$

where, P_i^t is the probability of selecting instance i at iteration t , and w_i^t represents the weight of the instance. The summation ensures that probabilities are normalized.

The weight w_i^t evolves dynamically which is represented in Eq.(37).

$$w_i^{t+1} = w_i^t \cdot \left(1 + \alpha \cdot \frac{\delta_i^t}{\max(\delta^t)}\right) \quad (37)$$

The term δ_i^t measures the contribution of instance i to the impurity reduction of the tree. This adaptive adjustment ensures that data contributing to better splits are prioritized.

Feature subset selection for splitting nodes

The selection of feature subsets further enhances diversity. A stochastic selection

mechanism determines the subgroup for each node split, expressed as Eq.(38).

$$F_k^t = \{f: f \sim P(f) \wedge |F_k| \leq m\} \quad (38)$$

The set F_k^t includes features sampled probabilistically based on their importance scores $P(f)$, ensuring the subset size does not exceed m . The importance score $P(f)$ for feature f is computed dynamically as shown in Eq.(39).

$$P(f) = \frac{\exp(\lambda \cdot S_f)}{\sum_{j=1}^F \exp(\lambda \cdot S_j)} \quad (39)$$

where, S_f is the feature score, and λ adjusts the sensitivity to feature importance.

Adaptive Tree Depth Control

The depth of each tree is dynamically optimized to balance complexity and diversity. The adaptive depth d_t of a tree at iteration t is determined as Eq.(40).

$$d_t = d_{max} \cdot \left(1 - \frac{\phi \cdot t}{T}\right) \quad (40)$$

where, d_{max} is the maximum depth, ϕ is a decay parameter, and T is the total number of iterations. This equation ensures deeper trees initially for exploration and shallower ones later for convergence.

The stopping condition for tree growth at depth d uses an entropy threshold which is expressed in Eq.(41).

$$\epsilon_d = H_d - H_{min} \quad (41)$$

If $\epsilon_d < \tau$, tree growth halts at that node. Here, H_d represents the entropy at depth d , and H_{min} is the minimum entropy threshold.

Node splitting criterion for diversity

Each tree uses unique criteria for node splitting, leveraging an adaptive gain function is expressed in Eq.(42).

$$G_k^t = \alpha \cdot IG_k + \beta \cdot VR_k - \gamma \cdot GINI_k \quad (42)$$

The term G_k^t represents the gain for node k at iteration t , combining information gain (IG), variance reduction (VR), and Gini index ($GINI$). The weights α, β , and γ ensure flexibility across trees.

Random perturbations for tree diversity

To further enhance diversity, random perturbations are introduced during tree construction. The perturbation vector for node criteria is defined as Eq.(43).

$$\Delta\theta_k = \sigma \cdot R_k \quad (43)$$

where, $\Delta\theta_k$ is the perturbation for node k , σ is the scaling factor, and R_k is a random vector. This ensures that even similar trees exhibit variations in their decision-making paths.

Weighted contribution of trees

The contribution of each tree to the final ensemble prediction is weighted based on its performance during training is represented mathematically in Eq.(44).

$$W_t = \frac{1}{1 + \exp(-\kappa \cdot Acc_t)} \quad (44)$$

Here, W_t is the weight for tree t , κ regulates the influence of accuracy, and Acc_t denotes the accuracy of the tree on the validation subset.

Swarm-inspired feedback for tree refinement

Feedback from neighbouring trees influences the construction of new trees, creating a collaborative swarm-like dynamic. The feedback adjustment for tree t is expressed as Eq.(45).

$$\phi_t = \phi_{t-1} + \eta \cdot (\Phi_{best} - \Phi_{t-1}) \quad (45)$$

where, ϕ_t is the feedback parameter, Φ_{best} represents the best feedback observed, and η is the adjustment rate. This iterative feedback ensures continuous improvement in tree diversity and performance.

3.7. Optimization of Tree Depth in SO-RF

The optimization of tree depth in SO-RF employs adaptive strategies inspired by seal behaviour to balance complexity and performance. The process ensures trees are neither too shallow, which may underfit the data, nor too deep, which may overfit. This optimization improves model generalization and computational efficiency while maintaining diversity across trees.

Adaptive depth control mechanism

The depth of each tree is dynamically adjusted based on iteration and data complexity. The depth control function is expressed as Eq.(46).

$$d_t = d_{max} - \left\lceil \frac{\zeta \cdot t}{T} \right\rceil \quad (46)$$

where, d_t represents the depth of the tree at iteration t , d_{max} is the maximum allowable depth, ζ is the depth decay rate, and T is the total number of iterations. This function reduces tree depth progressively, ensuring initial exploration and later exploitation.

Entropy-based depth threshold

The entropy at each depth is computed to assess the information richness of splits is expressed in Eq.(47).

$$H_d = - \sum_{c=1}^C p_c \ln(p_c) \quad (47)$$

where, H_d represents the entropy at depth d , p_c is the proportion of samples in class c , and C is the number of classes. A threshold ϵ_d is defined as Eq.(48).

$$\epsilon_d = H_d - H_{min} \quad (48)$$

If ϵ_d falls below a predefined limit, tree growth at that depth halts, preventing unnecessary splits.

Depth optimization objective

An optimization function combines accuracy, diversity, and computational cost to determine the optimal depth as expressed in Eq.(49).

$$O_d = \alpha \cdot Acc_d + \beta \cdot D_d - \gamma \cdot C_d \quad (49)$$

where, O_d is the optimization objective at depth d , Acc_d represents accuracy, D_d is a diversity metric, C_d is the computational cost, and α, β , and γ are weights balancing these factors.

Penalty for over-depth

A penalty function discourages excessive depth that may lead to overfitting. The penalty term is defined as Eq.(50).

$$P_d = \rho \cdot (d - d_{opt})^2 \quad (50)$$

where, P_d is the penalty for depth d , ρ controls the severity of the penalty, and d_{opt} is the empirically derived optimal depth. This penalty is integrated into the optimization function to guide depth selection.

Adaptive gain adjustment

An adaptive gain adjustment ensures optimal splits at each depth. The adjusted gain function is mathematically represented in Eq.(51).

$$G_d = IG_d + \frac{v}{1 + \exp(-\tau \cdot (d_{max} - d))} \quad (51)$$

The term G_d represents the gain at depth d , IG_d is the information gain, v is a scaling parameter, and τ adjusts the rate of gain adaptation. This ensures deeper nodes focus on significant splits.

Swarm-inspired feedback for depth adjustment

Feedback from previously constructed trees influences depth decisions. The feedback-adjusted depth is expressed as Eq.(52).

$$d_{t+1} = d_t + \eta \cdot (\bar{d} - d_t) \quad (52)$$

where, d_{t+1} is the updated depth for the next tree, d_t is the current depth, \bar{d} is the average depth of

constructed trees, and η is a feedback adjustment factor. This encourages convergence to an optimal depth across trees.

Dynamic sample distribution

The distribution of samples across nodes at each depth impacts depth optimization. The distribution factor is given as Eq.(53).

$$\delta_d = \frac{|X_d|}{|X|} \quad (53)$$

where, δ_d is the proportion of samples at depth d , $|X_d|$ is the number of samples at depth d , and $|X|$ is the total number of samples. High δ_d at deeper nodes triggers adjustments to maintain balance.

Computation-efficiency metric

A metric evaluating computational efficiency at each depth is defined as expressed in Eq.(54).

$$C_d = \frac{\sum_{n=1}^{N_d} Comp(n)}{N_d} \quad (54)$$

where, C_d is the average computational cost at depth d , $Comp(n)$ is the cost for node n , and N_d is the total number of nodes at depth d . This metric ensures tree depth decisions are considered to be efficient.

3.8. Hyperparameter Fine-Tuning

Hyperparameter fine-tuning is crucial for optimizing the performance of the SO-RF model. This process uses seal-inspired optimization strategies to adjust parameters such as the number of trees, maximum depth, minimum samples per split, and feature subset size. The approach ensures these parameters align with the dataset and task requirements, enhancing predictive performance and generalization.

Search space definition

The fine-tuning process begins with defining the hyperparameter search space. Upper and lower limits bound each parameter. The search space for a hyperparameter h is represented as Eq.(55).

$$H = \{h: h_{min} \leq h \leq h_{max}\} \quad (55)$$

where, H denotes the set of possible values for h , while h_{min} and h_{max} are its lower and upper bounds, respectively.

The initial position of a candidate solution in the search space is randomized as expressed in Eq.(56).

$$h_i^{(0)} = h_{min} + r \cdot (h_{max} - h_{min}) \quad (56)$$

where, $h_i^{(0)}$ represents the initial value of the i -th hyperparameter, and r is a uniform random variable between 0 and 1.

Objective function for hyperparameter tuning

The objective function evaluates the performance of a hyperparameter combination. The evaluation metric, such as accuracy or F1-score, is computed as defined in Eq.(57).

$$F(H) = \frac{1}{k} \sum_{j=1}^k Eval(H, X_j, Y_j) \quad (57)$$

where, $F(H)$ is the average evaluation score across k -fold cross-validation, where X_j and Y_j are the training and validation datasets for fold j , and $Eval(H, X_j, Y_j)$ computes the score for a specific hyperparameter set H .

Dynamic exploration-exploitation balance

The exploration and exploitation phases are balanced dynamically during fine-tuning. The exploration probability $P_e^{(t)}$ at iteration, t is modelled as Eq.(58).

$$P_e^{(t)} = P_{min} + (P_{max} - P_{min}) \cdot exp\left(-\frac{t}{\tau}\right) \quad (58)$$

where, $P_e^{(t)}$ is the probability of exploring new areas of the search space, P_{min} and P_{max} are the minimum and maximum exploration probabilities, and τ controls the decay rate.

The exploitation probability complements exploration and is expressed mathematically in Eq.(59).

$$P_x^{(t)} = 1 - P_e^{(t)} \quad (59)$$

Adaptive step size for fine-tuning

Step size adaptation ensures efficient convergence during hyperparameter optimization. The step size $\Delta h_i^{(t)}$ for the i -th hyperparameter at iteration, t is defined as Eq.(60).

$$\Delta h_i^{(t)} = \eta \cdot \frac{\delta F(H)}{\partial h_i} \quad (60)$$

where, η is the learning rate, and $\frac{\delta F(H)}{\partial h_i}$ is the gradient of the objective function concerning h_i . This ensures that adjustments are proportional to the influence of each hyperparameter. The updated value of h_i is calculated as expressed in Eq.(61).

$$h_i^{(t+1)} = h_i^{(t)} + \Delta h_i^{(t)} \quad (61)$$

Diversity in hyperparameter solutions

To maintain diversity among candidate solutions, a perturbation factor is introduced as mathematically expressed in Eq.(62)

$$h_i^{(t+1)} = h_i^{(t)} + \sigma \cdot r \quad (62)$$

where, σ controls the perturbation magnitude, and r is a random vector. This prevents premature convergence to suboptimal solutions.

Penalty for overfitting

To discourage overfitting, a penalty term is incorporated into the objective function which is expressed mathematically in Eq.(63).

$$F'(H) = F(H) - \lambda \cdot Complexity(H) \quad (63)$$

where, $F'(H)$ is the penalized objective function, λ is the penalty coefficient, and $Complexity(H)$ measures the complexity of the model for the given hyperparameter set.

Collaborative search using seal-inspired behaviour

The fine-tuning process leverages collaborative search, mimicking seal swarm behaviour. The position of a candidate solution in the search space is updated as shown in Eq.(64).

$$h_i^{(t+1)} = h_i^{(t)} + \zeta \cdot (h_g - h_i^{(t)}) + \xi \cdot R \quad (64)$$

where, h_g is the global best solution, ζ is the attraction coefficient, ξ controls random exploration, and R is a random vector. This mechanism ensures convergence to the optimal hyperparameter values.

3.9. Diversity Maximization in SO-RF

Diversity maximization is a critical step in SO-RF to ensure each tree contributes unique insights to the ensemble. Incorporating seal-inspired behaviour enhances the exploration of the solution space, prevents redundancy among trees, and improves generalization. Diversity maximization addresses variability in feature selection, sample subsets, and decision paths, creating a robust and balanced Random Forest.

Quantifying diversity across trees

Diversity is measured by assessing differences in decision paths between trees. The pairwise diversity metric for trees T_i and T_j is expressed as Eq.(65).

$$D(T_i, T_j) = 1 - \frac{Sim(T_i, T_j)}{MaxSim} \quad (65)$$

where, $D(T_i, T_j)$ represents the diversity between two trees, $Sim(T_i, T_j)$ measures the similarity of their predictions, and $MaxSim$ is the maximum

possible similarity. Higher $D(T_i, T_j)$ indicates greater diversity.

The aggregate diversity across the forest is defined as Eq.(66).

$$D_{forest} = \frac{2}{N(N-1)} \sum_{i=1}^{N-1} \sum_{j=i+1}^N D(T_i, T_j) \quad (66)$$

where, D_{forest} represents the average diversity among N trees. This ensures the assessment encompasses all pairwise combinations.

Feature space dispersion

To enhance diversity, feature dispersion within the forest is maximized. Dispersion is defined as Eq.(67).

$$\Delta F = \frac{\sum_{k=1}^m \|F_k - \bar{F}\|}{m} \quad (67)$$

where, ΔF measures the dispersion of feature subsets across m trees, F_k is the feature set of tree k , and \bar{F} is the mean feature set vector. Higher dispersion ensures broader feature exploration.

Sample variability across trees

Sample variability is introduced by adjusting weights dynamically during bootstrap sampling. The weight of a sample x_i in tree k is defined as Eq.(68).

$$w_{i,k} = \frac{1}{1 + \exp(-k, \delta_{i,k})} \quad (68)$$

where, $w_{i,k}$ is the weight of sample i in tree k , κ regulates the sigmoid steepness, and $\delta_{i,k}$ measures the distance of x_i from the centroid of the samples in tree k .

Normalized weights are used to maintain consistency which is expressed mathematically in Eq.(69).

$$\hat{w}_{i,k} = \frac{w_{i,k}}{\sum_{j=1}^{n_k} w_{j,k}} \quad (69)$$

This ensures that the weights of all samples within a tree sum to 1, facilitating probabilistic sampling.

Tree path variability

Tree path variability is introduced by incorporating randomness into node-splitting criteria. The adjusted gain function for a node in tree k is expressed as Eq.(70).

$$G_k = \alpha \cdot IG_k + \beta \cdot VR_k - \gamma \cdot GINI_k + \rho \cdot R_k \quad (70)$$

where, G_k represents the gain, α, β , and γ are weighting for information gain (IG_k), variance reduction (VR_k), and Gini index ($GINI_k$), respectively, while ρ controls the influence of the random vector R_k . This mechanism introduces stochasticity into tree construction.

Diversity-conscious pruning

Pruning strategies ensure trees remain diverse by selectively retaining nodes that contribute to variability. The pruning metric for a node n in tree k is defined as Eq.(71).

$$P_k(n) = \frac{\Delta D(n)}{Cost(n)} \quad (71)$$

where, $P_k(n)$ represents the pruning priority, $\Delta D(n)$ measures the diversity gain from retaining the node, and $Cost(n)$ evaluates the computational cost of the node. Nodes with higher $P_k(n)$ are retained to maximize diversity.

Adaptive depth variation

Depth variation across trees is achieved by dynamically adjusting the maximum depth d_k for each tree k is expressed mathematically in Eq.(72).

$$d_k = d_{min} + \xi \cdot \sin\left(\frac{\pi \cdot k}{N}\right) \quad (72)$$

where, d_k is the depth of tree k , d_{min} is the minimum allowable depth, and ξ is the scaling factor. This ensures variability in tree complexity, further enhancing diversity.

Collaborative feedback for diversity

Seal-inspired feedback mechanisms enable collaborative adjustment of tree parameters. The feedback-adjusted weight for tree k is given as expressed in Eq.(73).

$$\Phi_k = \Phi_k^{prev} + \eta \cdot (D_{forest} - \Phi_k^{prev}) \quad (73)$$

where, Φ_k is the feedback-adjusted weight for tree k , Φ_k^{prev} is its previous value, D_{forest} is the aggregate diversity, and η is the learning rate for feedback incorporation.

3.10. Weighted Voting Mechanism

The weighted voting mechanism in SO-RF integrates the outputs of diverse trees to produce a robust and accurate final prediction. Inspired by seal-like decision-making behaviour, weights are assigned to individual trees based on their reliability and performance. This ensures that trees contributing significantly to predictive accuracy have a higher impact on the ensemble decision while maintaining robustness against noisy or redundant contributions.

Individual tree contribution

The contribution of each tree to the final prediction is evaluated using a reliability score. The score for tree T_k is defined as Eq.(74).

$$R_k = \frac{Acc_k}{\sum_{j=1}^N Acc_j} \quad (74)$$

where, R_k is the reliability score of tree T_k , Acc_k represents its accuracy on a validation

set, and N is the total number of trees. The normalization ensures all scores sum to 1.

Weighted voting for classification

For classification tasks, the weighted voting mechanism computes the class probabilities for each label c is expressed mathematically in Eq.(75).

$$P(c) = \sum_{k=1}^N R_k \cdot p_k(c) \quad (75)$$

where, $P(c)$ is the ensemble probability for class c , $p_k(c)$ does tree predict the probability T_k for c , and R_k is the tree's reliability score. This equation combines predictions while emphasizing trees with higher reliability.

The final predicted class is obtained which is mathematically represented in Eq.(76).

$$y = \underset{c}{\operatorname{argmax}} P(c) \quad (76)$$

The class y with the highest ensemble probability $P(c)$ is selected as the final prediction.

Weighted averaging for regression

For regression tasks, the ensemble prediction \hat{y} is calculated as a weighted average of individual tree predictions as expressed in Eq.(77).

$$\hat{y} = \sum_{k=1}^N R_k \cdot y_k \quad (77)$$

where, \hat{y} is the ensemble's prediction, y_k is the prediction of tree T_k , and R_k is the reliability score. This ensures that the final output reflects the contributions of reliable trees.

Diversity-based weight adjustment

The reliability score R_k is adjusted to incorporate tree diversity. The adjusted weight W_k for tree T_k is expressed as Eq.(78).

$$W_k = R_k \cdot (1 + \delta \cdot D_k) \quad (78)$$

where, W_k is the weight of tree T_k , δ is a scaling parameter, and D_k is the diversity score of the tree. This adjustment ensures that diverse trees are prioritized in the ensemble decision.

The diversity score D_k is computed as expressed in Eq.(79).

$$D_k = \frac{1}{N-1} \sum_{j \neq k} D(T_k, T_j) \quad (79)$$

where, D_k represents the average diversity of tree T_k relative to all other trees, and $D(T_k, T_j)$ measures pairwise diversity.

Confidence-based weighting

A confidence measure is integrated into the voting mechanism to reflect the reliability of

tree predictions. The confidence-adjusted weight Φ_k for tree T_k is defined as Eq.(80).

$$\Phi_k = W_k \cdot \frac{\operatorname{Conf}_k}{\sum_{j=1}^N \operatorname{Conf}_j} \quad (80)$$

where, Φ_k is the confidence-adjusted weight, and Conf_k represents the confidence of tree T_k in its predictions. This ensures predictions from confident trees are given higher priority.

Penalization for incorrect predictions

To mitigate the influence of trees with frequent errors, a penalization term is incorporated into the weight calculation which is expressed mathematically in Eq.(81).

$$W'_k = \Phi_k \cdot \exp(-\beta \cdot E_k) \quad (81)$$

where, W'_k is the penalized weight for tree T_k , β is a penalization coefficient, and E_k represents the error rate of tree T_k on a validation set. This adjustment reduces the impact of unreliable trees.

Adaptive voting threshold

An adaptive threshold τ_k is applied to filter out trees with low reliability which is represented mathematically in Eq.(82).

$$\tau_k = \frac{\mu_k}{1 + \sigma_k} \quad (82)$$

where, τ_k is the threshold for tree T_k , μ_k is its mean accuracy, and σ_k is the standard deviation of its performance across validation folds. Trees with weights below the threshold are excluded from voting.

3.11. Iterative Improvement in SO-RF

Iterative improvement is a crucial step in the SO-RF algorithm, enhancing the overall performance of the ensemble through progressive refinements. Inspired by the adaptive learning behaviour of seals, this step focuses on optimizing individual tree parameters, adjusting feature subsets, and refining weight distributions across iterations. The ensemble becomes more accurate and robust by iteratively analyzing feedback and making targeted improvements.

Refinement of feature subsets

Feature subsets used in individual trees are iteratively refined to enhance their relevance and diversity. The refinement is guided by the weighted contribution of each feature to the ensemble's accuracy, expressed as Eq.(83).

$$w_f^{(t+1)} = w_f^{(t)} + \eta \cdot \left(\frac{\operatorname{Acc}_f}{\sum_{i=1}^F \operatorname{Acc}_i} \right) \quad (83)$$

where, $w_f^{(t+1)}$ is the updated weight of feature f at iteration $t+1$, η is the learning rate, and Acc_f represents the contribution of feature f to the

accuracy of the ensemble. This ensures features with higher utility are prioritized in future iterations.

Dynamic tree parameter adjustment

Tree-specific parameters are adjusted iteratively to enhance individual performance. The adjustment for the maximum depth $d_k^{(t+1)}$ of tree, k is calculated as Eq.(84).

$$d_k^{(t+1)} = d_k^{(t)} + \alpha \cdot \left(\frac{Gain_k}{\sum_{j=1}^N Gain_j} \right) \quad (84)$$

where, $d_k^{(t+1)}$ is the updated depth, α is the scaling factor, and $Gain_k$ represents the average gain achieved by tree k . This adjustment balances tree complexity and performance.

Adaptive weight distribution

Weights assigned to trees in the ensemble are iteratively refined to improve prediction reliability. The updated weight $W_k^{(t+1)}$ for tree k is defined as Eq.(85).

$$W_k^{(t+1)} = W_k^{(t)} \cdot \left(1 + \beta \cdot \frac{\Delta Acc_k}{MaxAcc} \right) \quad (85)$$

where, $W_k^{(t+1)}$ is the refined weight, β controls the adjustment magnitude, ΔAcc_k is the improvement in accuracy for tree k , and $MaxAcc$ is the maximum accuracy observed.

Optimization of splitting criteria

The splitting criteria for nodes in each tree are refined iteratively based on feedback. The adjusted criterion for node n is calculated as Eq.(86).

$$C_n^{(t+1)} = C_n^{(t)} + \gamma \cdot \left(\frac{\Delta G_n}{\sum_{j=1}^{N_n} \Delta G_j} \right) \quad (86)$$

where, $C_n^{(t+1)}$ is the updated criterion, γ is a scaling parameter, ΔG_n represents the gain improvement for node n , and N_n is the total number of nodes in the tree. This ensures that nodes contributing more to performance receive higher priority.

Incorporation of feedback mechanisms

Feedback mechanisms inspired by seal behaviour guide iterative improvement by adjusting weights and parameters based on the performance of neighbouring trees. The feedback-adjusted parameter $P_k^{(t+1)}$ for tree, k is expressed as Eq.(87).

$$P_k^{(t+1)} = P_k^{(t)} + \delta \cdot (\bar{P}_k - P_k^{(t)}) \quad (87)$$

where, $P_k^{(t+1)}$ is the updated parameter, δ is the feedback adjustment rate, and \bar{P}_k is the average parameter value among neighbouring trees.

Diversity improvement across iterations

The dispersion of feature subsets across iterations is maximized to maintain and enhance diversity. The iterative update for feature dispersion $\Delta F^{(t+1)}$ is defined as Eq.(88).

$$\Delta F^{(t+1)} = \Delta F^{(t)} + \epsilon \cdot \left(\frac{Var(F^{(t)})}{MaxVar} \right) \quad (88)$$

Here, $\Delta F^{(t+1)}$ represents the updated dispersion, ϵ is the dispersion adjustment factor, $Var(F^{(t)})$ is the variance of feature subsets at iteration t , and $MaxVar$ is the maximum allowable variance.

Penalization of redundant trees

Redundant trees are penalized iteratively to prevent over-reliance on similar decision paths. The penalization factor $P_k^{(t+1)}$ for tree, k is expressed as Eq.(89).

$$P_k^{(t+1)} = P_k^{(t)} \cdot \exp(\zeta \cdot Red_k) \quad (89)$$

where, $P_k^{(t+1)}$ is the penalized factor, ζ is the penalization coefficient, and Red_k measures redundancy for tree k . This encourages unique contributions from each tree.

4. ABOUT DATASET AND METRICS

The OASIS (Open Access Series of Imaging Studies) Alzheimer's Detection Dataset is a well-structured collection of MRI scans, supporting research in cognitive decline and neurodegenerative disorders. This dataset consists of 1012 images, systematically divided into training and testing subsets for structured model evaluation. The training set comprises 796 images, while the testing set contains 216 images, ensuring balanced representation for algorithm development. The dataset includes T1-weighted MRI scans, offering high-resolution anatomical details of gray matter, white matter, and cerebrospinal fluid (CSF). Diagnostic labels categorize subjects into Normal Control (NC), Mild Cognitive Impairment (MCI), and Alzheimer's Disease (AD), allowing supervised classification models to distinguish between cognitive states. Additional attributes such as age, gender, and brain volume measurements provide insights into the progression of neurodegeneration. This dataset is ideal for machine learning and deep learning-based applications, including automated classification, early detection systems, and feature extraction models. The availability of well-labeled MRI scans supports advanced computational neuroscience research, improving clinical decision-making in Alzheimer's detection.

5. OUTCOMES AND DEBATES

Results and discussions involve analyzing the obtained performance metrics and interpreting their significance in relation to the classification framework. The effectiveness of a model is evaluated through multiple indicators, among which classification accuracy and F-measure hold primary importance. Classification accuracy represents the proportion of correctly classified instances among the total instances, providing a direct measure of the model’s reliability. The F-measure, or F-score, balances precision and recall, ensuring that both false positives and false negatives are adequately considered in assessing model performance.

Classification accuracy varies significantly among the evaluated models. The SO-RF model achieves a classification accuracy of 72.328%, outperforming INN-MT, which records an accuracy of 57.097%, and FDCNN-AS, which achieves 53.483%. This improvement highlights the effectiveness of the bio-inspired optimization strategy integrated into SO-RF, allowing it to refine feature selection and reduce classification errors. The increased true positive and true negative rates in SO-RF contribute to higher accuracy, indicating enhanced decision boundaries and better generalization in detecting Alzheimer’s Disease.

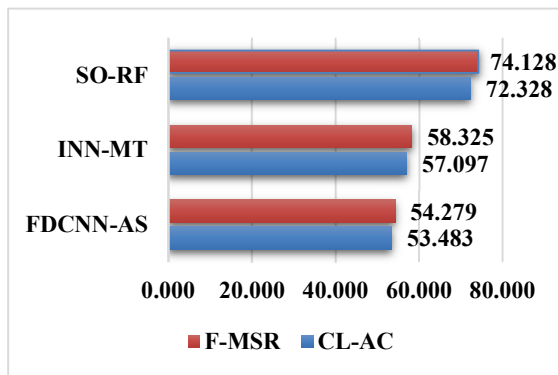


Fig2. Classification Accuracy and F-Measure

The F-measure further supports the superiority of SO-RF, which attains a value of 74.1282%, surpassing INN-MT at 58.3252% and FDCNN-AS at 54.279%. This metric considers both precision and recall, reinforcing the model’s ability to handle imbalanced data and minimize incorrect classifications. The notable increase in F-measure for SO-RF is attributed to its optimized classification framework, which efficiently balances sensitivity and specificity. The

performance gain confirms the impact of integrating bio-inspired optimization with Random Forest, leading to a more reliable and precise classification system for Alzheimer’s Disease detection.

Fig.2 further illustrates the comparative performance of the models concerning classification accuracy and F-measure. The significant gap between SO-RF and the other two models emphasizes the advantage of structured optimization techniques in enhancing classification performance. The findings validate the proposed approach, demonstrating its potential in improving automated Alzheimer’s Disease detection through advanced Machine Learning methodologies.

The Fowlkes-Mallows Index (FMI) and Matthews Correlation Coefficient (MCC) provide valuable insights into the quality of classification. The FMI evaluates the geometric mean of precision and recall, measuring the balance between correctly classified positive instances and overall predictions. The MCC, a comprehensive statistical metric, assesses the correlation between actual and predicted classifications, offering a more reliable evaluation for imbalanced datasets.

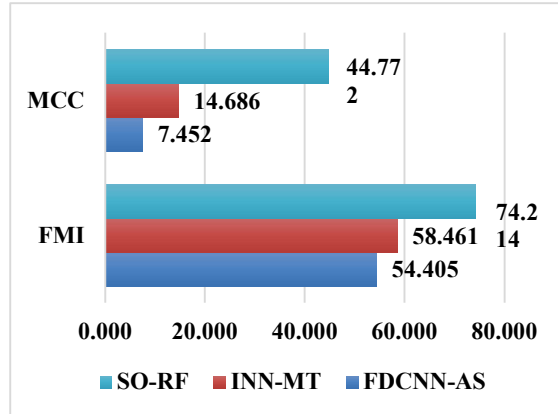


Fig3. FMI and MCC

The FMI values reveal a clear distinction in model performance. The SO-RF model achieves an FMI of 74.214, surpassing INN-MT at 58.461 and FDCNN-AS at 54.405. This improvement indicates that the SO-RF framework enhances both precision and recall, ensuring a well-balanced classification strategy. The higher FMI suggests that the bio-inspired optimization approach integrated into SO-RF refines feature selection and decision boundaries, minimizing misclassifications and improving overall predictive reliability.

The MCC values further validate the efficiency of SO-RF in handling classification

complexity. The SO-RF model records an MCC of 44.772, significantly higher than INN-MT at 14.686 and FDCNN-AS at 7.452. MCC considers all four confusion matrix components, making it a robust metric for evaluating model performance, particularly in datasets with class imbalances. The substantial improvement in SO-RF indicates better discrimination between Alzheimer's and non-Alzheimer's cases, reflecting an optimized classification structure.

Fig 3. exhibits the comparative evaluation of models with the parameters FMI and MCC. From the comparison that SO-RF consistently outperforms other models in FMI and MCC, confirming the effectiveness of integrating bio-inspired optimization with Random Forest. The findings reinforce the model's ability to enhance early detection and classification accuracy, making it a promising tool for Alzheimer's Disease diagnosis.

Among the critical indicators, precision and recall play a significant role in assessing the reliability of the model. Precision measures the proportion of correctly identified positive cases out of all predicted positive instances, highlighting the model's ability to minimize false positives. Recall, also known as sensitivity or the true positive rate, evaluates the proportion of correctly classified positive instances from the actual positive cases, reflecting the model's capacity to detect Alzheimer's cases accurately. The SO-RF model demonstrates a substantial improvement in precision, achieving 70.730%, compared to 54.600% in INN-MT and 50.825% in FDCNN-AS. This significant increase indicates that SO-RF effectively reduces false positives while maintaining high classification confidence. The enhancement results from optimized feature selection and decision boundary refinement, ensuring that the model prioritizes relevant features for accurate classification.

In recall, SO-RF outperforms the other models, reaching 77.869%, whereas INN-MT records 62.595% and FDCNN-AS attains 58.237%. The increased recall in SO-RF signifies its ability to correctly classify a higher proportion of actual positive cases, minimizing false negatives. This improvement stems from the bio-inspired optimization strategies embedded in SO-RF, enhancing sensitivity to critical Alzheimer's-related patterns in the dataset.

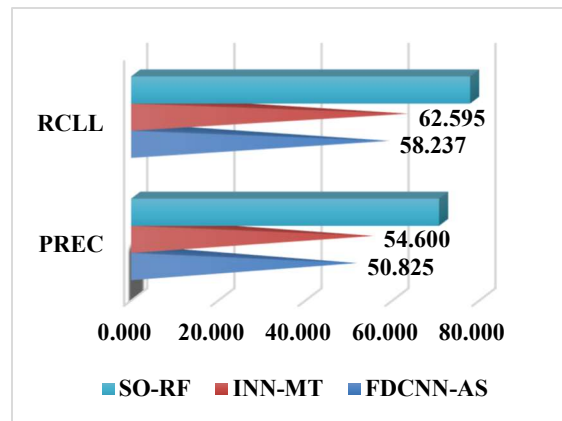


Fig4. Precision and Recall

Fig4. Illustrates the results obtained by models evaluated under the metrics Precision and Recall. The combined evaluation of precision and recall confirms that SO-RF achieves a more balanced classification performance, maintaining both specificity and sensitivity. The bio-inspired optimization incorporated into the model significantly enhances predictive accuracy, making it a more effective tool for Alzheimer's Disease classification. The results validate the potential of SO-RF in refining automated diagnostic frameworks, ensuring reliable and early detection of neurodegenerative conditions.

The SO-RF framework presents multiple advantages over existing models such as INN-MT and FDCNN-AS. It achieves superior classification accuracy, F-measure, FMI, and MCC through robust feature selection and bio-inspired optimization. However, it incurs higher computational costs and lacks real-time adaptability or privacy-preserving capabilities like those in federated systems. Interestingly, the integration of seal-inspired dynamics particularly in convergence, diversity, and feature-space exploration is a novel contribution in ensemble learning for Alzheimer's detection. These mechanisms enhance interpretability and decision reliability, positioning SO-RF as a promising, innovative tool in automated neurodegenerative disease diagnosis.

6. CONCLUSION

The proposed research introduces a novel classification framework SO-RF by integrating seal-inspired bio-optimization with Random Forest to enhance early detection of Alzheimer's Disease. This study contributes an innovative multi-layered

optimization strategy, impacting feature selection, sampling, tree construction, and voting mechanisms, which collectively improve model interpretability, precision, and generalization. The incorporation of adaptive convergence dynamics, diversity maximization, and iterative refinement establishes SO-RF as a significant advancement over conventional ML and DL models. Comparative analysis confirms superior performance in accuracy, F-measure, FMI, MCC, precision, and recall, reinforcing the framework's robustness in handling imbalanced and high-dimensional neuroimaging data. In the current healthcare landscape, where early diagnosis and personalized interventions are imperative, the findings offer a timely and practical solution. The SO-RF model holds potential for integration into automated diagnostic tools, supporting clinicians in delivering informed, early-stage decisions for neurodegenerative conditions. This research lays a strong foundation for future developments in interpretable, optimization-driven, and scalable AI systems tailored for Alzheimer's Disease detection.

REFERENCES

- [1] L. Liu, S. Liu, L. Zhang, X. V. To, F. Nasrallah, and S. S. Chandra, "Cascaded Multi-Modal Mixing Transformers for Alzheimer's Disease Classification with Incomplete Data," *Neuroimage*, vol. 277, p. 120267, 2023, doi: <https://doi.org/10.1016/j.neuroimage.2023.120267>.
- [2] A. Asgharzadeh-Bonab, H. Kalbkhani, and S. Azarfardian, "An Alzheimer's disease classification method using fusion of features from brain Magnetic Resonance Image transforms and deep convolutional networks," *Healthcare Analytics*, vol. 4, p. 100223, 2023, doi: <https://doi.org/10.1016/j.health.2023.100223>.
- [3] M. Aparna and B. S. Rao, "Xception-Fractalnet: Hybrid Deep Learning Based Multi-Class Classification of Alzheimer's Disease," *Computers, Materials and Continua*, vol. 74, no. 3, pp. 6909–6932, 2022, doi: <https://doi.org/10.32604/cmc.2023.034796>.
- [4] C. Zhang, W. Fan, B. Wang, C. Chen, and H. Li, "Self-paced semi-supervised feature selection with application to multi-modal Alzheimer's disease classification," *Information Fusion*, vol. 107, p. 102345, 2024, doi: <https://doi.org/10.1016/j.inffus.2024.102345>.
- [5] C. Zhang, W. Fan, H. Li, and C. Chen, "Multi-level graph regularized robust multi-modal feature selection for Alzheimer's disease classification," *Knowl Based Syst*, vol. 293, p. 111676, 2024, doi: <https://doi.org/10.1016/j.knosys.2024.111676>.
- [6] Y. Dai *et al.*, "DE-JANet: A unified network based on dual encoder and joint attention for Alzheimer's disease classification using multi-modal data," *Comput Biol Med*, vol. 165, p. 107396, 2023, doi: <https://doi.org/10.1016/j.compbio.2023.107396>.
- [7] V. Viswan, F. Hajamohideen, K. Subramanian, N. Shaffi, and M. Mahmud, "6 - Enhancing insights: unravelling the potential of preprocessing MRI for artificial intelligence based Alzheimer's disease classification," in *Machine Learning Models and Architectures for Biomedical Signal Processing*, S. L. Tripathi, V. E. Balas, M. Mahmud, and S. Banerjee, Eds., Academic Press, 2025, pp. 125–151. doi: <https://doi.org/10.1016/B978-0-443-22158-3.00006-5>.
- [8] M. Zhang, L. Sun, Z. Kong, W. Zhu, Y. Yi, and F. Yan, "Pyramid-attentive GAN for multimodal brain image complementation in Alzheimer's disease classification," *Biomed Signal Process Control*, vol. 89, p. 105652, 2024, doi: <https://doi.org/10.1016/j.bspc.2023.105652>.
- [9] T. Mahmood, A. Rehman, T. Saba, Y. Wang, and F. S. Alamri, "Alzheimer's disease unveiled: Cutting-edge multi-modal neuroimaging and computational methods for enhanced diagnosis," *Biomed Signal Process Control*, vol. 97, p. 106721, 2024, doi: <https://doi.org/10.1016/j.bspc.2024.106721>.
- [10] Z. Hu, Y. Li, Z. Wang, S. Zhang, and W. Hou, "Conv-Swinformer: Integration of CNN and shift window attention for Alzheimer's disease classification," *Comput Biol Med*, vol. 164, p. 107304, 2023, doi: <https://doi.org/10.1016/j.compbio.2023.107304>.
- [11] K. Hansson *et al.*, "Corrigendum to 'Use of the tau protein-to-peptide ratio in CSF to improve diagnostic classification of Alzheimer's disease' [Clin. Mass Spectrom. 14 (Part B) (2019) 74–82]," *Journal of Mass Spectrometry and Advances in the Clinical Lab*, vol. 26, p. 35, 2022, doi: <https://doi.org/10.1016/j.jmsacl.2022.08.002>.
- [12] S. Venkat, T. Ghodeswar, P. Chavan, S. K. Narayanasamy, and K. Srinivasan, "MRI-

- based automated diagnosis of Alzheimer's disease using Alzh-Net deep learning model," *Biomed Signal Process Control*, vol. 102, p. 107367, 2025, doi: <https://doi.org/10.1016/j.bspc.2024.107367>.
- [13] A. Dong, G. Zhang, J. Liu, and Z. Wei, "Latent feature representation learning for Alzheimer's disease classification," *Comput Biol Med*, vol. 150, p. 106116, 2022, doi: <https://doi.org/10.1016/j.compbimed.2022.106116> [14] Z. Wang *et al.*, "Distance-weighted Sinkhorn loss for Alzheimer's disease classification," *iScience*, vol. 27, no. 3, p. 109212, 2024, doi: <https://doi.org/10.1016/j.isci.2024.109212>.
- [15] Y.-W. Bao *et al.*, "Combined Quantitative amyloid- β PET and Structural MRI Features Improve Alzheimer's Disease Classification in Random Forest Model - A Multicenter Study," *AcadRadiol*, vol. 31, no. 12, pp. 5154-5163, 2024, doi: <https://doi.org/10.1016/j.acra.2024.06.040>.
- [16] M. A. Maito *et al.*, "Classification of Alzheimer's disease and frontotemporal dementia using routine clinical and cognitive measures across multicentric underrepresented samples: a cross sectional observational study," *The Lancet Regional Health - Americas*, vol. 17, p. 100387, 2023, doi: <https://doi.org/10.1016/j.lana.2022.100387>.
- [17] T. Del Rosario Hernandez, N. R. Joshi, S. V. Gore, J. A. Kreiling, and R. Creton, "Combining supervised and unsupervised analyses to quantify behavioral phenotypes and validate therapeutic efficacy in a triple transgenic mouse model of Alzheimer's disease," *Biomedicine & Pharmacotherapy*, vol. 181, p. 117718, 2024, doi: <https://doi.org/10.1016/j.biopha.2024.117718>.
- [18] M. Nour, U. Senturk, and K. Polat, "A novel hybrid model in the diagnosis and classification of Alzheimer's disease using EEG signals: Deep ensemble learning (DEL) approach," *Biomed Signal Process Control*, vol. 89, p. 105751, 2024, doi: <https://doi.org/10.1016/j.bspc.2023.105751>.
- [19] V. P. Nithya, N. Mohanasundaram, and R. Santhosh, "An Early Detection and Classification of Alzheimer's Disease Framework Based on ResNet-50," *Curr Med Imaging*, vol. 20, 2024, doi: <https://doi.org/10.2174/1573405620666230825113344>.
- [20] M. Leming, S. Das, and H. Im, "Construction of a confounder-free clinical MRI dataset in the Mass General Brigham system for classification of Alzheimer's disease," *ArtifIntell Med*, vol. 129, p. 102309, 2022, doi: <https://doi.org/10.1016/j.artmed.2022.102309>.
- [21] A. Tiwari, S. Dhavamani, T. Patel, J. Ramasamy, and S. Gesing, "Abstract 2608: Comparative evaluation of deep transfer learning with learning-from-scratch for Alzheimer disease MRI images Classification," *Journal of Biological Chemistry*, vol. 299, no. 3, Supplement, p. 103449, 2023, doi: <https://doi.org/10.1016/j.jbc.2023.103449>.
- [22] A. Pérez-Millan *et al.*, "Beyond group classification: Probabilistic differential diagnosis of frontotemporal dementia and Alzheimer's disease with MRI and CSF biomarkers," *Neurobiol Aging*, vol. 144, pp. 1-11, 2024, doi: <https://doi.org/10.1016/j.neurobiolaging.2024.08.008>.
- [23] A. Parameswari, K. V. Kumar, and S. Gopinath, "Thermal analysis of Alzheimer's disease prediction using random forest classification model," *Mater Today Proc*, vol. 66, pp. 815-821, 2022, doi: <https://doi.org/10.1016/j.matpr.2022.04.357>.
- [24] J. Ramkumar, R. Karthikeyan, and V. Valarmathi, "Alpine Swift Routing Protocol (ASRP) for Strategic Adaptive Connectivity Enhancement and Boosted Quality of Service in Drone Ad Hoc Network (DANET)," *International Journal of Computer Networks and Applications*, vol. 11, no. 5, pp. 726-748, Sep. 2024, doi: [10.22247/ijcna/2024/45](https://doi.org/10.22247/ijcna/2024/45).
- [25] R. Karthikeyan and R. Vadivel, "Boosted Mutated Corona Virus Optimization Routing Protocol (BMCVORP) for Reliable Data Transmission with Efficient Energy Utilization," *Wirel Pers Commun*, 2024, doi: [10.1007/s11277-024-11155-7](https://doi.org/10.1007/s11277-024-11155-7).
- [26] M. Leela, K. Helenprabha, and L. Sharmila, "Prediction and classification of Alzheimer Disease categories using Integrated Deep Transfer Learning Approach," *Measurement: Sensors*, vol. 27, p. 100749, 2023, doi: <https://doi.org/10.1016/j.measen.2023.100749>.
- [27] T. Jo *et al.*, "Circular-SWAT for deep learning based diagnostic classification of Alzheimer's disease: application to metabolome data," *EBioMedicine*, vol. 97, p. 104820, 2023, doi: <https://doi.org/10.1016/j.ebiom.2023.104820>.
- [28] B. Wang, "Enhanced brain efficiency network by integrating the new causality with fMRI

- and its application for Alzheimer's Disease study," *Biomed Signal Process Control*, vol. 86, p. 105364, 2023, doi: <https://doi.org/10.1016/j.bspc.2023.105364>.
- [29] S. Ben Hassen, M. Neji, Z. Hussain, A. Hussain, A. M. Alimi, and M. Frikha, "Deep learning methods for early detection of Alzheimer's disease using structural MR images: a survey," *Neurocomputing*, vol. 576, p. 127325, 2024, doi: <https://doi.org/10.1016/j.neucom.2024.127325>.
- [30] H. Cheng *et al.*, "De-accumulated error collaborative learning framework for predicting Alzheimer's disease progression," *Biomed Signal Process Control*, vol. 89, p. 105767, 2024, doi: <https://doi.org/10.1016/j.bspc.2023.105767>.
- [31] T. Tuncer, S. Dogan, and A. Subasi, "FiboNeXt: Investigations for Alzheimer's Disease detection using MRI," *Biomed Signal Process Control*, vol. 103, p. 107422, 2025, doi: <https://doi.org/10.1016/j.bspc.2024.107422>.
- [32] L. S. Gill, J. Kaur, and N. Goel, "Machine learning and texture features based approach for classifying Alzheimer's disease," *Procedia Comput Sci*, vol. 235, pp. 2741–2748, 2024, doi: <https://doi.org/10.1016/j.procs.2024.04.258>.
- [33] M. Eslami, S. Tabarestani, and M. Adjouadi, "A unique color-coded visualization system with multimodal information fusion and deep learning in a longitudinal study of Alzheimer's disease," *ArtifIntell Med*, vol. 140, p. 102543, 2023, doi: <https://doi.org/10.1016/j.artmed.2023.102543>.
- [34] M. Abdelaziz, T. Wang, W. Anwaar, and A. Elazab, "Multi-scale multimodal deep learning framework for Alzheimer's disease diagnosis," *Comput Biol Med*, vol. 184, p. 109438, 2025, doi: <https://doi.org/10.1016/j.compbimed.2024.109438>.
- [35] J. L. Ávila-Jiménez, V. Cantón-Habas, M. del P. Carrera-González, M. Rich-Ruiz, and S. Ventura, "A deep learning model for Alzheimer's disease diagnosis based on patient clinical records," *Comput Biol Med*, vol. 169, p. 107814, 2024, doi: <https://doi.org/10.1016/j.compbimed.2023.107814>.
- [36] C. Ozdemir and Y. Dogan, "Advancing early diagnosis of Alzheimer's disease with next-generation deep learning methods," *Biomed Signal Process Control*, vol. 96, p. 106614, 2024, doi: <https://doi.org/10.1016/j.bspc.2024.106614>.
- [37] M. Nour, U. Senturk, and K. Polat, "A novel hybrid model in the diagnosis and classification of Alzheimer's disease using EEG signals: Deep ensemble learning (DEL) approach," *Biomed Signal Process Control*, vol. 89, p. 105751, 2024, doi: <https://doi.org/10.1016/j.bspc.2023.105751>.
- [38] M. Chakraborty, N. Naoal, S. Momen, and N. Mohammed, "ANALYZE-AD: A comparative analysis of novel AI approaches for early Alzheimer's detection," *Array*, vol. 22, p. 100352, 2024, doi: <https://doi.org/10.1016/j.array.2024.100352>.
- [39] J. Sheng *et al.*, "A hybrid multimodal machine learning model for Detecting Alzheimer's disease," *Comput Biol Med*, vol. 170, p. 108035, 2024, doi: <https://doi.org/10.1016/j.compbimed.2024.108035>.
- [40] S. Venkat, T. Ghodeswar, P. Chavan, S. K. Narayanasamy, and K. Srinivasan, "MRI-based automated diagnosis of Alzheimer's disease using Alzh-Net deep learning model," *Biomed Signal Process Control*, vol. 102, p. 107367, 2025, doi: <https://doi.org/10.1016/j.bspc.2024.107367>.
- [41] C. Zhang, W. Fan, H. Li, and C. Chen, "Multi-level graph regularized robust multi-modal feature selection for Alzheimer's disease classification," *Knowl Based Syst*, vol. 293, p. 111676, 2024, doi: <https://doi.org/10.1016/j.knosys.2024.111676>.
- [42] G. Biagetti, P. Crippa, L. Falaschetti, S. Luzzi, and C. Turchetti, "Classification of Alzheimer's Disease from EEG Signal Using Robust-PCA Feature Extraction," *Procedia Comput Sci*, vol. 192, pp. 3114–3122, 2021, doi: <https://doi.org/10.1016/j.procs.2021.09.084>.
- [43] R. Jaganathan and R. Vadivel, "Intelligent Fish Swarm Inspired Protocol (IFSIP) for Dynamic Ideal Routing in Cognitive Radio Ad-Hoc Networks," *International Journal of Computing and Digital Systems*, vol. 10, no. 1, pp. 1063–1074, 2021, doi: [10.12785/ijcds/100196](https://doi.org/10.12785/ijcds/100196).
- [44] P. Menakadevi and J. Ramkumar, "Robust Optimization Based Extreme Learning Machine for Sentiment Analysis in Big Data," in *2022 International Conference on Advanced Computing Technologies and Applications, ICACTA 2022*, 2022, doi: [10.1109/ICACTA54488.2022.9753203](https://doi.org/10.1109/ICACTA54488.2022.9753203).

- [45] J. Ramkumar, R. Vadivel, and B. Narasimhan, "Constrained Cuckoo Search Optimization Based Protocol for Routing in Cloud Network," *International Journal of Computer Networks and Applications*, vol. 8, no. 6, pp. 795–803, 2021, doi: 10.22247/ijcna/2021/210727.
- [46] S. P. Geetha, N. M. S. Sundari, J. Ramkumar, and R. Karthikeyan, "ENERGY EFFICIENT ROUTING IN QUANTUM FLYING AD HOC NETWORK (Q-FANET) USING MAMDANI FUZZY INFERENCE ENHANCED DIJKSTRA'S ALGORITHM (MFI-EDA)," *J Theor Appl Inf Technol*, vol. 102, no. 9, pp. 3708–3724, 2024, [Online]. Available: <https://www.scopus.com/inward/record.uri?eid=2-s2.0-85197297302&partnerID=40&md5=72d51668bee6239f09a59d2694df67d6>
- [47] M. P. Swapna, J. Ramkumar, and R. Karthikeyan, "Energy-Aware Reliable Routing with Blockchain Security for Heterogeneous Wireless Sensor Networks," in *Lecture Notes in Networks and Systems*, 2025, pp. 713–723. doi: 10.1007/978-981-97-6106-7_43.
- [48] J. Ramkumar, K. S. Jeen Marseline, and D. R. Medhunhashini, "Relentless Firefly Optimization-Based Routing Protocol (RFORP) for Securing Fintech Data in IoT-Based Ad-Hoc Networks," *International Journal of Computer Networks and Applications*, vol. 10, no. 4, pp. 668–687, 2023, doi: 10.22247/ijcna/2023/223319.
- [49] R. Jaganathan, S. Mehta, and R. Krishan, "Preface," *Intelligent Decision Making Through Bio-Inspired Optimization*, pp. xiii–xvi, 2024, [Online]. Available: <https://www.scopus.com/inward/record.uri?eid=2-s2.0-85192858710&partnerID=40&md5=f8f1079e8772bd424d2cdd979e5f2710>
- [50] K. S. J. Marseline, J. Ramkumar, and D. R. Medhunhashini, "Sophisticated Kalman Filtering-Based Neural Network for Analyzing Sentiments in Online Courses," in *Smart Innovation, Systems and Technologies*, 2024, pp. 345–358. doi: 10.1007/978-981-97-3690-4_26.
- [51] N. K. Ojha, A. Pandita, and J. Ramkumar, "Cyber security challenges and dark side of AI: Review and current status," in *Demystifying the Dark Side of AI in Business*, 2024, pp. 117–137. doi: 10.4018/979-8-3693-0724-3.ch007.
- [52] A. Senthilkumar, J. Ramkumar, M. Lingaraj, D. Jayaraj, and B. Sureshkumar, "Minimizing Energy Consumption in Vehicular Sensor Networks Using Relentless Particle Swarm Optimization Routing," *International Journal of Computer Networks and Applications*, vol. 10, no. 2, pp. 217–230, 2023, doi: 10.22247/ijcna/2023/220737.
- [53] J. Ramkumar and R. Vadivel, "Whale optimization routing protocol for minimizing energy consumption in cognitive radio wireless sensor network," *International Journal of Computer Networks and Applications*, vol. 8, no. 4, pp. 455–464, 2021, doi: 10.22247/ijcna/2021/209711.
- [54] M. P. Swapna and J. Ramkumar, "Multiple Memory Image Instances Stratagem to Detect Fileless Malware," in *Communications in Computer and Information Science*, 2024, pp. 131–140. doi: 10.1007/978-3-031-59100-6_11.
- [55] J. Ramkumar, A. Senthilkumar, M. Lingaraj, R. Karthikeyan, and L. Santhi, "OPTIMAL APPROACH FOR MINIMIZING DELAYS IN IOT-BASED QUANTUM WIRELESS SENSOR NETWORKS USING NM-LEACH ROUTING PROTOCOL," *J Theor Appl Inf Technol*, vol. 102, no. 3, pp. 1099–1111, 2024, [Online]. Available: <https://www.scopus.com/inward/record.uri?eid=2-s2.0-85185481011&partnerID=40&md5=bf0ff974ceabc0ad58e589b28797c684>
- [56] L. Mani, S. Arumugam, and R. Jaganathan, "Performance Enhancement of Wireless Sensor Network Using Feisty Particle Swarm Optimization Protocol," in *ACM International Conference Proceeding Series*, 2022. doi: 10.1145/3590837.3590907.
- [57] D. Jayaraj, J. Ramkumar, M. Lingaraj, and B. Sureshkumar, "AFSROP: Adaptive Fish Swarm Optimization-Based Routing Protocol for Mobility Enabled Wireless Sensor Network," *International Journal of Computer Networks and Applications*, vol. 10, no. 1, pp. 119–129, 2023, doi: 10.22247/ijcna/2023/218516.
- [58] M. Lingaraj, T. N. Sugumar, C. S. Felix, and J. Ramkumar, "Query aware routing protocol for mobility enabled wireless sensor network," *International Journal of Computer Networks and Applications*, vol. 8, no. 3, pp. 258–267, 2021, doi: 10.22247/ijcna/2021/209192.

- [59] J. Ramkumar and R. Vadivel, "Multi-Adaptive Routing Protocol for Internet of Things based Ad-hoc Networks," *Wirel Pers Commun*, vol. 120, no. 2, pp. 887–909, 2021, doi: 10.1007/s11277-021-08495-z.
- [60] J. Ramkumar and R. Vadivel, "Improved Wolf prey inspired protocol for routing in cognitive radio Ad Hoc networks," *International Journal of Computer Networks and Applications*, vol. 7, no. 5, pp. 126–136, 2020, doi: 10.22247/ijcna/2020/202977.
- [61] J. Ramkumar and R. Vadivel, "Improved frog leap inspired protocol (IFLIP) – for routing in cognitive radio ad hoc networks (CRAHN)," *World Journal of Engineering*, vol. 15, no. 2, pp. 306–311, 2018, doi: 10.1108/WJE-08-2017-0260.
- [62] J. Ramkumar, S. S. Dinakaran, M. Lingaraj, S. Boopalan, and B. Narasimhan, "IoT-Based Kalman Filtering and Particle Swarm Optimization for Detecting Skin Lesion," in *Lecture Notes in Electrical Engineering*, 2023, pp. 17–27. doi: 10.1007/978-981-19-8353-5_2.
- [63] R. Karthikeyan and R. Vadivel, "Proficient Dazzling Crow Optimization Routing Protocol (PDCORP) for Effective Energy Administration in Wireless Sensor Networks," in *IEEE International Conference on Electrical, Electronics, Communication and Computers, ELEXCOM 2023*, 2023. doi: 10.1109/ELEXCOM58812.2023.10370559.
- [64] R. Karthikeyan and R. Vadivel, "Boosted Mutated Corona Virus Optimization Routing Protocol (BMCVORP) for Reliable Data Transmission with Efficient Energy Utilization," *Wirel Pers Commun*, vol. 135, no. 4, pp. 2281–2301, 2024, doi: 10.1007/s11277-024-11155-7.
- [65] R. Jaganathan, S. Mehta, and R. Krishan, *Intelligent Decision Making Through Bio-Inspired Optimization*. 2024. doi: 10.4018/979-8-3693-2073-0.
- [66] J. Ramkumar, A. Senthilkumar, M. Lingaraj, R. Karthikeyan, and L. Santhi, "OPTIMAL APPROACH FOR MINIMIZING DELAYS IN IOT-BASED QUANTUM WIRELESS SENSOR NETWORKS USING NM-LEACH ROUTING PROTOCOL," *J Theor Appl Inf Technol*, vol. 102, no. 3, pp. 1099–1111, 2024, [Online]. Available: <https://www.scopus.com/inward/record.uri?eid=2-s2.0-85185481011&partnerID=40&md5=bf0ff974ceabc0ad58e589b28797c684>
- [67] S. P. Priyadharshini and J. Ramkumar, "Mappings Of Plithogenic Cubic Sets," *Neutrosophic Sets and Systems*, vol. 79, pp. 669–685, 2025, doi: 10.5281/zenodo.14607210.
- [68] S. P. Geetha, N. M. S. Sundari, J. Ramkumar, and R. Karthikeyan, "ENERGY EFFICIENT ROUTING IN QUANTUM FLYING AD HOC NETWORK (Q-FANET) USING MAMDANI FUZZY INFERENCE ENHANCED DIJKSTRA'S ALGORITHM (MFI-EDA)," *J Theor Appl Inf Technol*, vol. 102, no. 9, pp. 3708–3724, 2024, [Online]. Available: <https://www.scopus.com/inward/record.uri?eid=2-s2.0-85197297302&partnerID=40&md5=72d51668bee6239f09a59d2694df67d6>
- [69] R. Jaganathan, S. Mehta, and R. Krishan, "Preface," *Bio-Inspired Intelligence for Smart Decision-Making*, pp. xix–xx, 2024, [Online]. Available: <https://www.scopus.com/inward/record.uri?eid=2-s2.0-85195725049&partnerID=40&md5=7a2aa7adc005662eebc12ef82e3bd19f>
- [70] J. Ramkumar and R. Vadivel, "CSIP—cuckoo search inspired protocol for routing in cognitive radio ad hoc networks," in *Advances in Intelligent Systems and Computing*, 2017, pp. 145–153. doi: 10.1007/978-981-10-3874-7_14.
- [71] B. Suchitra, J. Ramkumar, and R. Karthikeyan, "FROG LEAP INSPIRED OPTIMIZATION-BASED EXTREME LEARNING MACHINE FOR ACCURATE CLASSIFICATION OF LATENT AUTOIMMUNE DIABETES IN ADULTS (LADA)," *J Theor Appl Inf Technol*, vol. 103, no. 2, pp. 472–494, 2025, [Online]. Available: <https://www.scopus.com/inward/record.uri?eid=2-s2.0-85217140979&partnerID=40&md5=9540433c16d5ff0f6c2de4b8c43a4812>
- [72] R. Jaganathan and V. Ramasamy, "Performance modeling of bio-inspired routing protocols in Cognitive Radio Ad Hoc Network to reduce end-to-end delay," *International Journal of Intelligent Engineering and Systems*, vol. 12, no. 1, pp. 221–231, 2019, doi: 10.22266/IJIES2019.0228.22.
- [73] J. Ramkumar, R. Karthikeyan, and M. Lingaraj, "Optimizing IoT-Based Quantum Wireless Sensor Networks Using NM-TEEN

- Fusion of Energy Efficiency and Systematic Governance,” in *Lecture Notes in Electrical Engineering*, 2025, pp. 141–153. doi: 10.1007/978-981-97-6710-6_12.
- [74] R. Jaganathan, S. Mehta, and R. Krishan, *Bio-Inspired intelligence for smart decision-making*. 2024. doi: 10.4018/9798369352762.
- [75] J. Ramkumar, V. Valarmathi, and R. Karthikeyan, “Optimizing Quality of Service and Energy Efficiency in Hazardous Drone Ad-Hoc Networks (DANET) Using Kingfisher Routing Protocol (KRP),” *International Journal of Engineering Trends and Technology*, vol. 73, no. 1, pp. 410–430, 2025, doi: 10.14445/22315381/IJETT-V73I1P135.
- [76] J. Ramkumar, B. Varun, V. Valarmathi, D. R. Medhunhashini, and R. Karthikeyan, “JAGUAR-BASED ROUTING PROTOCOL (JRP) FOR IMPROVED RELIABILITY AND REDUCED PACKET LOSS IN DRONE AD-HOC NETWORKS (DANET),” *J Theor Appl Inf Technol*, vol. 103, no. 2, pp. 696–713, 2025, [Online]. Available: <https://www.scopus.com/inward/record.uri?eid=2-s2.0-85217213044&partnerID=40&md5=e38a375e46cf43c95d6702a3585a7073>
- [77] J. Ramkumar, R. Karthikeyan, and V. Valarmathi, “Alpine Swift Routing Protocol (ASRP) for Strategic Adaptive Connectivity Enhancement and Boosted Quality of Service in Drone Ad Hoc Network (DANET),” *International Journal of Computer Networks and Applications*, vol. 11, no. 5, pp. 726–748, 2024, doi: 10.22247/ijcna/2024/45.
- [78] J. Ramkumar, C. Kumuthini, B. Narasimhan, and S. Boopalan, “Energy Consumption Minimization in Cognitive Radio Mobile Ad-Hoc Networks using Enriched Ad-hoc On-demand Distance Vector Protocol,” in *2022 International Conference on Advanced Computing Technologies and Applications, ICACTA 2022*, 2022. doi: 10.1109/ICACTA54488.2022.9752899.
- [79] R. Vadivel and J. Ramkumar, “QoS-enabled improved cuckoo search-inspired protocol (ICSIP) for IoT-based healthcare applications,” in *Incorporating the Internet of Things in Healthcare Applications and Wearable Devices*, 2019, pp. 109–121. doi: 10.4018/978-1-7998-1090-2.ch006.
- [80] A. Lakhan *et al.*, “FDCNN-AS: Federated deep convolutional neural network Alzheimer detection schemes for different age groups,” *Inf Sci (N Y)*, vol. 677, p. 120833, 2024, doi: <https://doi.org/10.1016/j.ins.2024.120833>.
- [81] X. Zhang, L. Gao, Z. Wang, Y. Yu, Y. Zhang, and J. Hong, “Improved neural network with multi-task learning for Alzheimer’s disease classification,” *Heliyon*, vol. 10, no. 4, p. e26405, 2024, doi: <https://doi.org/10.1016/j.heliyon.2024.e26405>.